Iron precipitation kinetics during microbial ferrous-ion oxidation

by

Kevin Nzuzi Swami

Thesis submitted in fulfilment of the requirements for the degree of

Master of Engineering: Chemical Engineering

In the Faculty of Engineering & the Built Environment

Cape Peninsula University of Technology Cape Town, South Africa

October 2024

CPUT copyright information

Supervisor

Prof. Tunde V Ojumu (PhD)

Professor and Head of Bioprocess and Environmental Engineering Research (BioPER)

Department of Chemical Engineering Faculty of Engineering and the Built Environment

Cape Peninsula University of Technology

Bellville Campus, Cape Town

Co-Supervisor

Dr. Babatunde Oladipo (DEng)

Research Fellow (Bioprocess and Environmental Engineering Research)

Department of Chemical Engineering Faculty of Engineering and the Built Environment

Cape Peninsula University of Technology

Bellville Campus, Cape Town

DECLARATION

I, **Kevin Nzuzi Swami**, declare that the contents of this thesis represent my own unaided work and that the thesis has not previously been submitted for academic examination towards any qualification. Furthermore, it represents my own opinions and not necessarily those of the Cape Peninsula University of Technology.

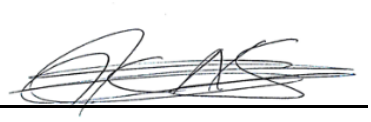

Signed

December, 2024

Date

ABSTRACT

The formation of ferric-ion precipitates, such as jarosite, has been extensively documented during the bioleaching process. These precipitates serve as pathways for unwanted iron to escape from the system in various processes. However, a significant accumulation over an extended period can hinder reaction kinetics and reduce the overall efficiency of bioleaching. Therefore, this study sought to investigate the kinetics of the ferric-ion precipitates that are formed through bacterial oxidation.

Experiments were conducted using a mixed mesophilic culture in shake flasks, with temperatures set at 30, 35, and 40 °C in a shaking incubator maintained at a constant pH of 1.7. The experiments lasted 14 days, with an agitating speed of 120 rpm. Upon analysing the quantification results, the maximum quantity of ferric-ion solid precipitates that developed was 2.48 grams at a temperature of 40 °C. Additionally, the data indicated that ferric-ion precipitation began 24 hours into the process.

The precipitates generated were characterized by dense, light ochreous yellow residues. The patterns created by the X-ray powder diffraction (XRD) of these crystals were identified as potassium jarosite (K-jarosite), with its chemical formula being [$KFe_3(SO_4)_2(OH)_6$]. The scanning electron microscopy (SEM) analysis of their shape showed clusters of spherical, oval, and/or rectangular, powdery particles, all without clear, sharp edges. The Fourier transform infrared (FTIR) spectra of these crystals revealed the vibrational frequencies of SO_4^{2-}, H_2O, OH, and Fe–O in the jarosite. Furthermore, the thermogravimetric analysis (TGA) tests indicated the loss of hydroxyl groups from K-jarosite and the complete decomposition of yavapaiite when heated.

The formation of ferric precipitates occurred according to first-order kinetics. The estimated activation energy was 117.2 kJ/mol with a frequency factor (K) of 2.94 X 10^{20} mmol $Fe^{3+}.h^{-1}$, indicating that the process was endothermic, with an average [Fe^{3+}] of threshold 1.22 g/L. The thermodynamic parameters obtained were entropy (ΔS) = 0.25 kJ/mol K, Gibbs free energy (ΔG) = 43.89, 42.64, and 41.39 kJ/mol at 30, 35, and 40 °C, respectively, and Enthalpy (ΔH) = 120 kJ/mol. These values suggest that the formation of ferric precipitates was non-spontaneous and required a considerable amount of energy to proceed towards spontaneity.

This study revealed that the generation of iron precipitation during microbial ferrous-ion oxidation by mesophilic consortia follows first-order kinetics. This process is endothermic and non-spontaneous, necessitating energy to transition to a spontaneous state. The findings could provide valuable insights for biohydrometallurgical processes aimed at managing and controlling jarosite formation and accumulation, thereby minimizing metal losses.

DEDICATION

This thesis is dedicated to my dearest mom Yvette Ntumba Kankienza; my sisters Dorcas Bapu, Christivie Lenvo, and my entire family for their unwavering support toward me and all their sacrifices.

ACKNOWLEDGMENT

First and foremost, I would like to give thanks to my Lord and Saviour Jesus Christ for enabling me to reach this stage in my life. I acknowledge that it was not by my strength nor abilities that I have achieved this, but his grace alone has led me to this achievement. I am not brighter than most people who are out there wishing to have this opportunity but for various reasons they are unable to.

I am very thankful to my supervisor, Prof. Tunde V. Ojumu, for allowing me to work under his guidance. The insights, expertise, and knowledge he contributed to my work have been invaluable.

Words alone would not suffice to express my gratitude toward Dr. Babatunde Oladipo for his constant support, motivation, and guidance. Being able to benefit from his knowledge and experience in the field enabled me to avoid making certain mistakes and learn fast as a result.

In my research, I thank the CPUT Centre for Postgraduate Studies (CPGS) for providing me with the postgraduate bursary.

I express my thanks to Ms. H. Small, Mr. A. Bester and Ms. G. Lentoor for their technical assistance throughout this study.

Special thanks to Axel Engo Mba and Dr. Joel Biyoghe for sheltering me during my first academic year as a postgraduate. It is remarkable the kindness, support, and love shown to me. Additionally, I would like to thank Thomas Ondo, Clotaire Eben Deng Essima, and Brice Ekome Nna for opening their home to me and being wonderful brothers to me.

I thank the Light of the World Cell group for being an amazing family to me. Through this cell group, I have experienced what unconditional love as mentioned in the scriptures, feels and looks like.

My sincerest gratitude goes out to the pastorate, ministers, and members of Christ Vision Church for their prayers and affection.

For their support and sacrifices during this journey, I am thankful to Rachel ‘Chel’, Caleb, Jultanie and Noela ‘Zoe’.

I am thankful to have the support of Merveille Tolela, Patricia N. Thsibasu, Franken Elenga, Diane Mbongo, Bedan Kambamba, Sarah Elenga Bonana, Christopher Ipiengo and Jacky Mouyecket throughout my academic journey. Your friendship has grown into a family and I am blessed to have you.

I am grateful to my friends and fellow postgraduates for their support and assistance during this journey. The conversations and advice were helpful especially in those moments when going forward seemed to be impossible. To Clive Griffith, Magan Ross, Evral Ntsa, Vinny Katambwe, Jennifer Oraegbunam, Walu Kaira, Shaun Mgoma, Whitney Heuvel, and Zilungile Mqoqi. You are all greatly appreciated.

I am thankful to my partner Merveille Nda Ngalela for her love and unwavering support in this journey. She always believed in me and my vision of things. Additionally, I also thank her family for being very welcoming to me.

LIST OF PUBLICATION AND PRESENTATION

Conference Proceedings

Swami, K.N., Oraegbunam, J.C., Oladipo, B. & Ojumu, T. V. (2024). Microbial Dynamics : Occurrence of Dominant Strains during Bio-oxidation of Ferrous Ion. *Proceedings of the 63rd Conference of Metallurgists, COM 2024* (Springer), https://doi.org/10.1007/978-3-031-67398-6_181

Oral Presentations

Swami, K. N. & Ojumu, T. V. (2022). Kinetics of ferric-ion precipitation: implication on their metal sorption. Interinstitutional Chemical Engineering Postgraduate Symposium 2022, Stellenbosch, South Africa, 30 September 2022

Swami, K. N. & Ojumu, T. V. (2023). Kinetics of Iron Precipitation in a Microbial-mediated Ferrous-ion Oxidation. Bioprocessing Symposium 2023, Johannesburg, South Africa, 8 August 2023

Swami, K. N. & Ojumu, T. V. (2023). Kinetics of biogenic iron precipitation in a ferrous-ion bio-oxidation system. Minerals Research Showcase 2023 Conference, Cape Town, South Africa, 13 - 14 November 2023

TERMS AND CONCEPTS CITED

Biohydrometallurgy: Low-grade ores can be processed using this eco-friendly and cost-efficient form of hydrometallurgy.

Bioleaching: A key part of biohydrometallurgy is bioleaching, which utilises specific properties of bacteria and archaea to extract metals from their sulphide ores.

Bio-oxidation: Bio-oxidation represents a pivotal sub-process within the bioleaching operation. This thesis places significant emphasis on microbial ferrous-ion oxidation.

Bacteria/Archaea: These microorganism species, primarily composed of iron- and sulphur-oxidizing organisms, are predominantly employed in bio-oxidation and bioleaching processes. They are primarily classified into three categories: mesophiles, moderately thermophiles, and extreme thermophiles.

Continuous stirred tank reactor: A Continuous Stirred Tank Reactor (CSTR) is a type of reactor designed to facilitate the ideal mixing of reactants, including the growth medium and the bacterial culture. Concurrently, the product of the reaction, in this case, the iron precipitate, is also present within the reactor.

Heap bioleaching: This method, which involves irrigation-based leaching, is preferred due to its energy-saving and cost-effective nature, making it an ideal approach for processing substantial volumes of low-grade ores.

Iron precipitation: This delineates a process or phenomenon within biohydrometallurgical process streams, wherein unwanted iron components are typically removed through oxidation to Fe^{3+}, subsequently followed by the hydrolysis-precipitation of an iron compound.

Jarosite: Jarosite is a significant compound associated with passivation and/or the formation of iron precipitates. The fundamental formula for jarosite-type compounds is $AFe_3(SO_4)_2(OH)_6$, where *A* represents various species, including H_3O^+, Na^+, K^+, $NH4^+$, among others.

Mesophilic bacteria: These microorganisms are the most prevalent in the process of bioleaching, which involves the oxidation of iron and sulphur, and are typically found at temperatures below 40 °C, which are considered optimal for their activity.

Table of Contents

LIST OF FIGURES

LIST OF TABLES

Chapter 1: Introduction

1.1 Background

Bioleaching is an economical process for recovering metals by using living organisms such as bacteria (Tekin & Yoruk, 2013; Roy & Roy, 2015), and the process requires little operating costs and initial investment (Abdollahi et al., 2019). Various bioleaching techniques have been developed for mineral extraction, tailored to the ore grade. These techniques include heap bioleaching for low-grade ores and concentrates, stirred tank bioleaching for finely ground flotation concentrates, and irrigated dump leaching for low-grade ores from mines (Ojumu, 2008; Mabusela, 2017). It is utilized in processing hard-to-treat gold ores before cyanidation and in which case it is referred to as biooxidation, and also in the recovering copper from secondary copper sulphide ores within the mining industry

Bioleaching is primarily driven by microbial ferrous-iron oxidation. Many industrially important sulphide minerals require ferric-ion as a key reagent for oxidation (Ojumu, 2008). Microbial ferrous-ion oxidation is completed by a series of cyclic processes that include both direct and indirect reactions. Ferrous ions (Fe^{2+}) are converted to ferric ions (Fe^{3+}) by microorganisms in acidic environments (Dopson et al., 2007), as well as the conversion of sulphur compounds to sulphur or sulphates. The ferric-ion (Fe^{3+}) that results is an oxidising agent that acts as a lixiviant in the oxidation of metal sulphides, while the reduced ferrous-ion (Fe^{2+}) is replenished by indirect processes in a cyclic bioleaching process (Mazuelos et al., 2001). However, when the Fe^{3+} ion is formed, iron (III) hydroxides and other ferric complexes, such as jarosite, are generated (Plumb et al., 2008).

Different forms of iron precipitates are formed when ferrous ions are oxidised in the bioleaching process (Nazari et al., 2014). A variety of operations benefit from these precipitates by providing a channel for unwanted iron to escape the circuit (Kaksonen et al., 2014). Precipitation takes place under controlled conditions within traditional hydrometallurgical processes, resulting in the formation of relatively well-defined compounds like goethite, crystalline jarosite, or hematite (Gramp et al., 2008; Mabusela, 2017), bioleaching, for example, occurs in less regulated circumstances, where a mix of different iron compounds forms, including schwertmannite, ferric hydroxides, jarosites, and oxyhydroxides (Gramp et al., 2008; Roger & Herbert, 1997). In biological systems, ferric-ion precipitation is orders of magnitude greater than in chemical and abiotic systems (Mabusela, 2017).

The occurrence of precipitates has been documented in various studies on oxidation and bioleaching of ferrous ions by microorganisms. According to Chukwuchendo and Ojumu (2017), as ferrous-ion oxidation occurred simultaneously with ferric-ion precipitation, ferric-ion

precipitation followed a first-order rate law; moreover, the rate constants increased as the operating temperature increased. Ahonen & Tuovinen (1989), Kupka et al. (2007), and Chukwuchendo (2016) found that during active oxidation, cultures that oxidised ferrous-ion at low temperatures were free of precipitates, however, precipitates were only observed after months of operation. Although precipitation can be reduced significantly under cold conditions, Oladipo et al. (2021) stated that considerable build-up of precipitate over a lengthy period can impede kinetics and limit bioleaching effectiveness by occluding desirable metals inside the precipitate residue.

The extensive characterization of ferric-ion precipitates has been explored, focusing primarily on their chemical composition, physical properties, and mineralogy (Kaksonen et al., 2014; Mabusela, 2017). Sorption studies were done by Oladipo et al. (2021) because it has been reported that precipitates limit the efficiency of bioleaching by adsorbing the desired minerals, such as copper. According to Oladipo et al. (2021), precipitates exhibit chemisorption through an ion-exchange mechanism as their primary adsorption mechanism. However, there are limited or no reported studies that focus on ferric-ion precipitation kinetics. In addition, there is no information on whether minimum and maximum Fe^{3+} concentrations exist in the solution necessary for precipitates to start forming.

The purpose of this research is to understand how temperature affects the kinetics of ferric-ion precipitates. This knowledge will allow for a better understanding of the ferric-ion precipitation kinetics and an indication of how to reduce ferric-ion precipitation by adjusting solution temperature, as well as a strategy for operating/designing bioleaching and ferrous biooxidation processes that minimise base metal loss.

1.2 Research Hypothesis and Questions

This study examined the following hypotheses and questions:

Hypothesis 1: In the bioleaching process, precipitation is unavoidable. As a result, a certain number of ferric ions would be present in the solution before they start to precipitate.

- Does precipitation occur continuously if there is a sufficient amount of ferric ions present in the solution for it to start?

Hypothesis 2: Temperature and pH significantly influence the rate of ferric ion precipitation.

- Is there a certain temperature at which precipitation is favoured, and how do the temperature changes affect precipitation kinetics?

1.3 Research Objectives

The objectives of this study are outlined below:

- To investigate the effect of operating temperature on the kinetics of ferric-ion precipitation.
- To determine whether there is a threshold concentration of ferric-ion for precipitation to occur.
- To estimate the energetic and thermodynamic parameters involved in the formation of iron precipitate during the bio-oxidation process.

1.4 Significance of the study

This study's findings will help prevent metal losses and provide knowledge of precipitate management and control in a typical bioleaching heap. The study will further aid in the control of process parameters in a typical bioleaching heap, so that iron precipitate can be minimised, increasing bioleaching efficiency, and reducing precipitate interference on desired metal extraction kinetics.

1.5 Thesis outline

The thesis is divided into six chapters as follows.:

Chapter 1 contains an overview of the research background, the problem statement, and the research objectives, which describe the aim of the study. Additionally, there are brief comments of previous research and conclusions about ferric-ion precipitation. Finally, there is a brief explanation of the relevance of this current investigation.

Chapter 2 contains a comprehensive analysis of existing relevant literature.

Chapter 3 describes the experimental setup, as well as the operating and analytical methodologies used. Moreover, it describes the experimental technique, the material, and the bacterial culture and growth media used in this study.

Chapter 4 presents the experimental data and analysis of the investigation. The chapter focuses on the impact of temperature on the precipitates formed by ferric ions. Furthermore, the chapter also determines the kinetics and thermodynamics of ferric-ion precipitate formation.

Chapter 5 of the thesis contains the characterisation study of the generated ferric-ion precipitates.

Chapter 6 of the thesis summarizes the research findings and offers recommendations for future work.

Chapter 7 contains a reference list outlining the sources used in this study.

Chapter 2: Literature review

2.1 Bioleaching

2.1.1 Historical background

The principles governing bioleaching have been used since antiquity, albeit without understanding them (Kazadi, 2007; Mabusela, 2017). The Chinese are thought to have been the first to perform bioleaching, maybe even before any other country, between 100 and 200 BC. They used a procedure said to have been created by mediaeval Chinese alchemists to commercialise this technology for copper manufacturing (Rawlings, 2002; Mabusela, 2017). As with many biotechnological processes, these methods may have been employed since prehistoric times, according to Bosecker (1997) and the Greeks and Romans likely recovered copper from mined water more than 2000 years ago. There's evidence that ancient people figured out how to recover copper that had been bioleached naturally. One example may be discovered during the Roman Empire or at Rio Tinto, Spain, in the 18th century, wherein copper was allegedly retrieved from acidic waters (Gentina & Acevedo, 2016).

A natural process was believed to be involved in the bioleaching at Rio Tinto mines, and the river was named Rio Tinto, which means dark-coloured, because of its reddish colour caused by the high concentration of dissolved ferric-ion (Chowdhury, 2012). Even though leaching sulfidic copper ores has a rich history, it wasn't until the 20th century that scientists found out about the involvement of bacteria in this process. Until the mid-17th century, bacteria had not been discovered, which explains why this discovery was so late century (Rawlings, 2002; Mabusela, 2017).

The development of this biotechnology, however, began about 1950, when microorganisms engaged in copper leaching were discovered and described. It was this foundational information that paved the way for a more complete understanding of the relationship between this unique microbial activity and copper dissolution and its potential as a copper recovery technique (Gentina & Acevedo, 2016).

The recovery of metals from low-grade ores and concentrates that are not economically recoverable using traditional methods is on the rise, thanks to microbial leaching technologies. However, it's important to note that bacteria play a crucial role in enriching metals in water from mineral deposits and mines, a discovery that has only been made in the past 50 years. The method of dissolving substances is referred to as bioleaching, and it occurs naturally in areas where the right conditions are favourable for the growth of the ubiquitous bioleaching bacteria (Bosecker, 1997). In 1980, copper leaching from heaps was the first commercial use of biohydrometallurgy, which was developed to enhance microorganism activity. Between

1980 and 1996, the Lo Aguirre mine in Chile used bioleaching to treat 16,000 tonnes per day (Olson et al., 2003). The first commercial facility dedicated to the pre-treatment of refractory gold-containing concentrates was inaugurated at the Fairview operation in South Africa during the mid-1980s, which marked the start of biohydrometallurgy's expansion into other metals recovery (Brierley & Brierley, 2001).

For a long time, bioleaching was assumed to be a method for recovering metals from flotation tailings, waste, and low-grade ores. Bioleaching is now used as the primary procedure in large-scale copper mining operations and as a critical pre-treatment step in the processing of refractory gold ores (Acevedo, 2000).

According to Brierley (2008), bioleaching from heap sites makes up approximately 7% of the global total of 17 million tonnes of copper output. If dump bioleaching is taken into account, bioleaching accounts for an extra 13-18% of global copper output. Bio-hydrometallurgical processing (Bioleaching-Solvent Extraction-Electrowinning) accounts for around 20-25 per cent of global copper output today (Panda et al., 2015).

2.1.2 The mechanism of bioleaching

Silverman and Ehrlich were the first to suggest the idea of bioleaching sulphide minerals (Ojumu, 2008). According to one description, bioleaching is a mixed chemical and microbiological process with ferric-ion and/or protons serving as the main reactants. Microorganisms are primarily used in the microbial oxidation of ferrous ions to produce or renew the leaching agents as well as to promote the reaction by establishing reaction spaces where the leaching occurs (Chowdhury, 2012). According to studies, the exopolysaccharide (EPS) layer, which acts as the reaction zone, is where bioleaching processes take place when microorganisms bind to metal surfaces (Ojumu, 2008; Chowdhury, 2012).

It has been studied and documented that mineral bioleaching procedures involve chemical and microbial oxidation reactions, with ferric-ion and protons serving as some of the reactants of the leaching reaction, according to (Ojumu et al., 2006; Wanjiya, 2013; Chukwuchendo, 2016). These processes include: (i) the chemical reaction of bacteria of reduced ferrous to ferric-ion, (ii) the chemical assault of sulphide minerals with ferric-ions, and (iii) the conversion of elemental sulphur to sulphuric acid.

$$2MS + 4Fe^{3+} \rightarrow 2M^{2+}\ 4Fe^{2+} + 2S^{0} \quad 2.1$$

$$4Fe^{2+} + O_2 + 4H^{+} \rightarrow 4Fe^{3+} + 2H_2O \quad 2.2$$

$$2S^{0} + 3O_2 + 2H_2O \rightarrow 2SO_4^{2-} + 4H^{+} \quad 2.3$$

In Equation 2.1 ferric-ion combines chemically with sulphide minerals to form a ferrous ion. Iron-oxidizing microorganisms regenerate ferric ions by oxidizing ferrous-ion to ferric-ions (Equation 2.2), enabling the leaching reaction in Equation 2.1 to continue cyclically. Sulphur-oxidizing bacteria convert sulphur species to sulphuric acid (see Equation 2.3) (Chowdhury, 2012; Wanjiya, 2013). These three important reactions in bioleaching are well depicted in Figure 2.1.

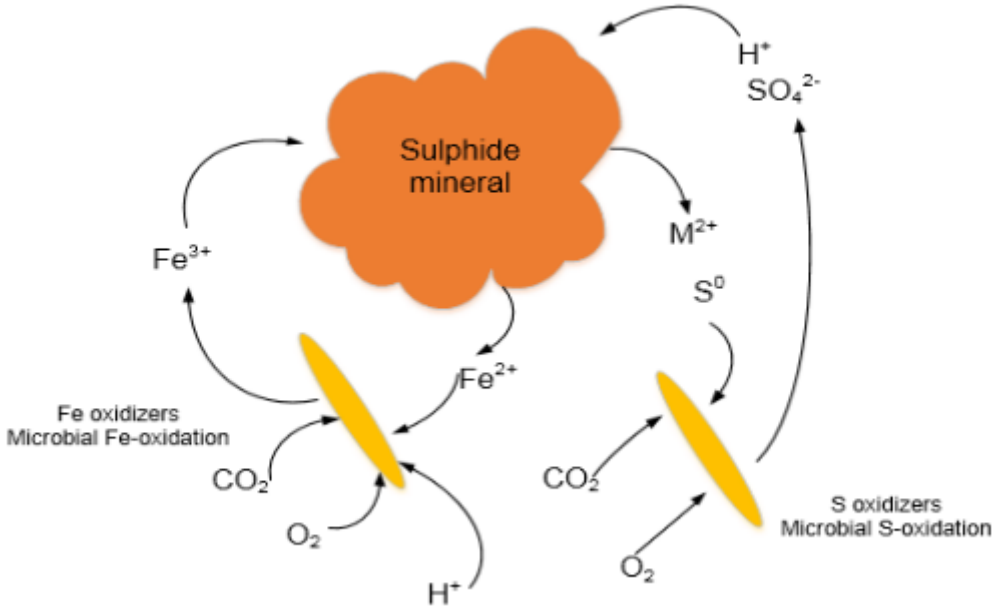

Figure 2.1: Schematic representation of the mechanism of bioleaching by Chukwuchendo (2016) modified after Hansford & Vargas (2001).

Sulphide minerals can be indirectly or directly leached by bacteria to release metals (Bosecker, 1997).

2.1.2.1 Direct Bioleaching

There is direct contact between microorganisms and a particular part of the mineral surface, but not with the entire surface. Electrochemical interactions are responsible for metal solubilization. When cells come into contact with suspended mineral particles, they adsorb them within minutes or hours. This enables microorganisms to grow and heavy metals to be leached simultaneously. Although this technique is simple to perform, it can be limited by dissolved metal ions that influence microbial metabolism and growth during the bioleaching process (Leahy et al., 2005; Anjum et al., 2012) (Fig. 3.4.1b).

According to Bosecker (1997) direct bacterial oxidation happens according to the following reactions:

$$4FeS_2 + 14O_2 + 4H_2O \xrightarrow{\text{bacteria}} 4FeSO_4 + 4H_2SO_4 \qquad 2.4$$

$$4FeSO_4 + O_2 + 2H_2SO_4 \xrightarrow{\text{bacteria}} 2Fe_2(SO_4)_3 + 2H_2O \quad 2.5$$

Here is a brief description of pyrite's direct bacterial oxidation:

$$4FeS_2 + 15O_2 + 2H_2O \xrightarrow{\text{bacteria}} 2Fe_2(SO_4)_3 + 2H_2SO_4 \quad 2.6$$

2.1.2.2 Indirect Bioleaching

A fungal or bacterial strain generates organic and inorganic acids as part of this mechanism. The process of bioleaching involves two stages. In the first step, process-active metabolites for leaching are produced by microorganisms that have been given the opportunity to grow in a suitable medium under suitable culture conditions. The second step involves leaching the mineral using the utilised culture medium under adverse leaching conditions (low pH, high temperature, etc.) in the absence of growing microorganisms. As a result, the metal is removed faster. Due to the direct physical interaction between microorganisms and the surface of the mineral, the direct method is frequently preferred over the indirect process (Mulligan et al., 2004; Szubert et al., 2006; Anjum et al., 2012) (Fig. 3.4.1a).

The following reaction can be used to explain indirect bioleaching (Bosecker, 1997):

$$MeS + Fe_2(SO_4)_3 \rightarrow MeSO_4 + 2FeSO_4 + S^o \quad 2.7$$

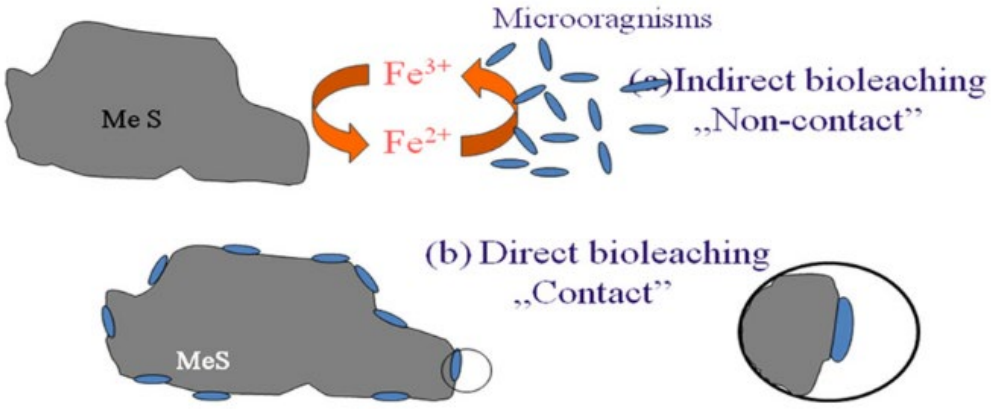

Figure 2.2: Direct and Indirect bioleaching mechanism by Anjum et al. (2012) modified after Crundwell (2003).

2.2 The microorganisms involved in bioleaching

It is common to find Iron-oxidizing bacteria such as Acidithiobacillus ferrooxidans in sites influenced by mining, these bacteria and archaea are phylogenetically diverse. (Hallberg and Johnson, 2001; Norris, 2007). These bacteria break down a broad variety of sulphide minerals,

releasing iron (and various other metals) and sulfo-oxyanions into the solution, and can assist in solving problems related to acid mine drainage (Rohwerder et al., 2003).

Microorganisms are crucial in the extraction of minerals from ores. They also have an impact on the kinetics of reactions in bioleaching procedures. They are acidophilic in nature and may survive in acidic environments. They may also oxidise ferrous-ion (Fe^{2+}) to ferric-ion (Fe^{3+}) in the presence of ambient carbon dioxide and oxygen, as well as oxidise elemental sulphur to sulphuric acid (H_2SO_4) (Kahrizi et al., 2009; Chukwuchendo, 2016).

Among the major functions of acidophilic microorganisms is the oxidation of ferrous-ions to ferric-ions and of sulphur ions to sulphuric acids (Das et al., 1999). They can grow in inorganic media with low pH values and tolerate metals with high ion concentrations. The resultant product (Fe^{3+}) is a chemical oxidant used in acidic mine effluent procedures to remove hydrogen sulphide from sour gases (Kahrizi et al., 2009). In this process, hydrogen sulphide is produced through two steps: the chemical oxidation of sulphide by Fe^{3+}, followed by the bacterial regeneration of Fe^{3+} as a leaching agent (Yujian et al., 2007).

Acidianus, Thiobacillus, Leptospirillium, and Sulfolobus are acidophilic bacteria with a dynamic influence on the oxidation of Fe^{2+} to Fe^{3+} and sulphur to H_2SO_4. Acidianus species are spherical with lobes that are formed like tetrahedrons, pyramid discs, or saucers. Thiobacillus species are rod-shaped, gram-negative, non-spore producing, and mesophilic, with the exception of Thermophilic Thiobacilli, which can thrive at higher temperatures (Das et al., 1999). While Leptospirillium species are spiral-shaped, non-spore forming, and gramme negative, Sulfobacillus species are gramme positive, rod-shaped with tapered ends, and can thrive at higher temperatures (Das et al., 1999).

As various microbe species function at different temperatures (Plumb et al., 2002; Franzmann et al., 2005; Jafari et al., 2019), microorganisms may be classified into three major categories depending on their temperature of activity, as follows: Extreme thermophilic, Mesophilic, and Moderate thermophilic (Bosecker, 1997; Jafari et al., 2019).

2.2.1 Mesophilic

The Mesophile species thrive best at room temperatures varying from 25°C to 40°C. Thiobacillus ferrooxidans is the most frequently widely utilised strain in the mesophilic family (Das et al., 1999). The optimal pH for these mesophilic microorganisms' development parameters is between 1.5 and 2.5. However, the mesophile Leptospirilium ferriphilium is also commonly utilised in the continuous bioleaching process. It has an optimal temperature of 38.6°C, can thrive at extremely low pH values, and can endure high ferric-iron concentrations

in the bioleaching solution (Franzmann et al., 2005). As such, its properties are comparable to those of Leptospirilium ferrooxidans (Wanjiya, 2013).

2.2.2 Moderate thermophilic

Some members of the newly established Sulfobacillus genus exhibit moderate thermophilic characteristics, while others retain their original codenames (Kazadi, 2007; Mabusela, 2017). Temperatures range from 400°C to 600°C for the growth of these bacteria. A gram-positive bacterium isolated from mineral waste dumps and biomining activities, sulphurobacillus is an endospore-forming bacteria. They may develop both autotrophically and heterotrophically. During their autotrophic growth, as electron sources, these bacteria use iron-bound sulphur compounds and/or sulphide minerals. Nevertheless, their ability to repair CO_2 is limited (Rawlings, 2002; Mabusela, 2017).

2.2.3 Extreme thermophilic

According to Rawlings (2005), there are fewer publications on the sorts of microorganisms found in mineral treatment operations which operate at temperatures above 700 °C. Furthermore, he also observed that archaea dominate these consortia rather than bacteria. Archaea have been discovered to thrive in temperatures as high as 900 °C, and at low temperatures by feeding on reduced sulphur. They have been claimed to be Acidianus species, such as A.dinfernus. The contribution of these organisms to industrial bioleaching remains unknown (Rawlings, 2005; Mabusela, 2017).

2.2.4 General characteristics of microorganisms

According to Ojumu (2008), the majority of microorganisms involved in mineral sulphide bioleaching are those responsible for generating the sulphuric acid and ferric ions essential for the leaching processes. They are chemolithotrophic bacteria and archaea that oxidise iron and sulphur. Although these microorganisms require a range of temperatures for optimal performance and are utilized in various processes, they possess several characteristics that make them particularly well-suited for their function in mineral solubilization:

- By absorbing CO_2 from the environment, they grow autotrophically,
- They generate energy by utilizing either ferrous ions or reduced inorganic sulphur compounds (or both) as electron donors, with oxygen serving as the electron acceptor,
- They are acidophiles, thriving in environments with low pH levels (typically ranging from 1.4 to 1.6), and
- They exhibit tolerance to a broad spectrum of metal ion concentrations, with this trait varying both within and between different species (Rawlings, 2002; Dopson et al., 2003).

It is consequently critical for optimal recovery of desirable metals from low-grade mineral sulphide ore concentrates that the microorganisms participating in the bioleaching process work at or near their optimum. This is only possible if the operational requirements for a specific microbial species participating in a specific bioleaching process are followed. If the operating requirements are not satisfied, the bioleaching process will be very sluggish, and the operation may be cancelled entirely (Wanjiya, 2013).

Table 2.1: The characteristics and physiological features of several microorganisms involved in bioleaching have been reported (Panda et al., 2015).

Strain (arranged alphabetically)	Shape	Optimum pH	Optimum Temp. (°C)	Capable of oxidation				Mode of nutrition for growth
				Pyrite	MS other than pyrite	Sulphur	Fe (II)	
Acidianus brierleyi	Irregular cocci	1.5–2.0	70	Y	Y	Y	Y	FA/FM
Acidianus infernus	Irregular cocci	2.0	90	Y	Y	Y	Y	Autotrophic
Acidianus sulfidivorans	Irregular cocci	0.35–3.0	74	Y	Y	Y	Y	Autotrophic
Acidiferrobacter thiooxidans	Rods	2.0	38	Y	NA	Y	Y	Autotrophic
Acidimicrobium ferrooxidans	Rods	2.0	45–50	Y	NA	N	Y	FA/FM
Acidiphilium cryptum	Rods	3	35–41	N	NA	Y	N	FH
Acidiplasma cupricumulans	Rods	1–1.2	54	NA	Y	Y	Y	FA/FM
Acidithiobacillus allbertensis	Rods	3.5–4.0	25–30	N	Y	Y	N	Autotrophic
Acidithiobacillus caldus	Rods	2.0–2.5	45	Y	Y	Y	Y	Autotrophic
Acidithiobacillus ferrivorans	Rods	2.5	27	Y	Y	Y	Y	Autotrophic
Acidithiobacillus ferrooxidans	Rods	2.5	30–35	N	Y	Y	N	Autotrophic
Acidithiobacillus thiooxidans	Rods	2.0–3.0	28–30	Y	NA	Y	Y	FA/FM
Alicyclobacillus disulfidooxidans	Rods	1.5–2.5	35	Y	NA	Y	Y	FA/FM
Alicyclobacillus GSM	Rods	1.8	47	Y	NA	Y	Y	FA/FM
Alicyclobacillus tolerans	Rods	2.5	37	Y	Y	Y	Y	FA/FM
Ferrimicrobium acidiphilum	Rods	2	35	Y	NA	N	Y	Heterotrophic
Ferrithrix thermotolerans	Filaments (occasionally single rods)	1.8	43	Y	NA	N	Y	Heterotrophic
Ferroplasma acidarmanus	Pleomorphic (irregular cocci or comma)	1.2	42	Y	NA	N	Y	Mixotroph
Ferroplasma acidiphilum	Pleomorphic (irregular cocci or comma)	1.7	35	Y	NA	N	Y	FA/FM
Leptospirillum ferriphilum	Spiral	1.3–1.8	30–37	Y	Y	N	Y	Autotrophic
Leptospirillum ferrooxidans	Spiral	1.5–3.0	28–30	Y	Y	N	Y	Autotrophic
Metallosphaera hakonensis	Lobe-shaped cocci	3.0	70	NA	Y	Y	NA	FA/FM
Metallosphaera prunae	Regular or slightly	2.0–3.0	75	Y	Y	Y	Y	FA/FM
Metallosphaera sedula	Irregular lobed cocci	2.0–3.0	75	Y	Y	Y	Y	FA/FM
Picrophilus torridus	Irregular lobed cocci	0.7	60	N	LI	N	N	Heterotrophic
Sulfobacillus acidophilus	Rods	2.0	45–50	Y	Y	Y	Y	FA/FM
Sulfobacillus benefaciens	Rods	1.5	39	Y	NA	Y	Y	FA/FM
Sulfobacillus sibiricus	Rods	2.2–2.5	55	Y	Y	Y	Y	FA/FM
Sulfobacillus thermosulfidooxidans	Rods	2.0	45–48	Y	Y	Y	Y	FA/FM
Sulfobacillus thermotolerans	Slightly curved rods	2.0–2.5	40	Y	Y	Y	Y	FA/FM
Sulfolobus acidocaldarius	Irregular cocci	2.0–3.0	70–75	Y/N	Y/N	N	N	FA
Sulfolobus metallicus	Irregular cocci	2.0–3.0	65	Y	Y	Y	Y	FA/FM
Sulfolobus solfataricus	Spherical	3.0–4.5	85	Y/N	Y/N	N	Y/N	Mixotroph
Sulfolobus tokodaii	Irregular cocci	2.5–3.0	80	N	NA	Y	N	Mixotroph
Sulfolobus yangmingensis	Irregular cocci	4	80	NA	Y	Y	NA	FA/FM
Sulphurococcus mirabilis	Irregular cocci	2.0–2.6	70–75	Y	Y	Y	Y	FA/FM
Sulphurococcus yellowstonensis	Irregular cocci	2.0–2.6	60	Y	Y	Y	Y	FA/FM
Thermoplasma acidophilum	Irregular shape due to the absence of a cell wall	1.0–2.0	59	N	NA	N	N	Heterotrophic
Thermoplasma volcanium	Irregular shape due to the absence of a cell wall	2.0	59–60	N	NA	N	N	Heterotrophic
Thiomonas cuprina	Rods	3.5–4.0	30–36	N	Y	Y	N	FA/FM

2.3 The application of bioleaching techniques

Biohydrometallurgy, an industrial application of bio-based processes, traditionally categorizes its methods into two primary processes: bioleaching and mineral bio-oxidation. Bioleaching is focused on dissolving base metals like nickel, copper, and zinc while mineral bio-oxidation is designed to free precious metals, typically silver and gold, that are "trapped" or "occluded" within sulphide minerals such as arsenopyrite and pyrite. Although bioleaching and mineral bio-oxidation are primarily used for copper, nickel, gold, and silver recovery, these techniques are increasingly being applied to extract additional metalloids and metals, and are being developed to treat non-sulphide ores (Brierley & Brierley, 2013).

Cobalt is also produced on a commercial basis in Uganda by bioleaching cobaltiferous pyrite concentrates (Morin & D'Hugues, 2007). The bioleaching of base metal sulphides, including lead (Pb), zinc (Zn), copper (Co), molybdenum (Mo), gallium (Ga), and nickel (Ni), as well as sulphide minerals that encase platinum-group metals, holds considerable potential. In the near future, nickel is likely to become the next major application for bioleaching base metals. Billiton has pioneered the BioNICID method, a biohydrometallurgical technique for extracting nickel from low-grade sulphide ores. However, the commercial viability of this method depends on successfully recovering nickel from the leach solution (Brierley & Brierley, 2001; Kazadi, 2007).

Today, bioleaching and mineral biooxidation are utilised in two main designed applications: stirred tanks and heaps. These methods have been used in mining for over 100 years for metal processing, but by the mid-1980s, they had been significantly adapted and enhanced for biohydrometallurgical processing (Brierley & Brierley, 2013).

2.3.1 Heap bioleaching

Heap bioleaching is a mineral processing technique in which low-grade ores are crushed, agglomerated, layered, and deposited on an impermeable pad that acts as the heap's foundation. The pad not only inhibits leach solution loss but also contamination of both the leaching solution and the earth. The pad is made up of clay as the bedding layer and a permeable drainage system comprised of a network of drainage pipes. Before mounting the ores on the prepared pad for leaching, the heaps are watered from the top with either sulphuric acid or an appropriate irrigation solution. This step is taken to prevent the segregation of particles of different sizes (Brierley & Brierley, 2001).

This method is mostly utilised for fine-grained ores that cannot be concentrated using flotation. Leaching takes place in enormous basins that may hold up to 12000 tonnes of ore. The process is comparable to dump leaching. Pipes are strategically inserted into heaps during

construction in some heap-leaching processes to supply sufficient oxygen to the deepest regions of the heap (Bosecker, 1997). Heap bioleaching is a highly designed process that is governed by particle size and ore grade/type. As opposed to dumping leaching methods, which have irregularly sized particles and are not planned, the heap bioleaching method makes more efficient recovery of metals from low-grade ores by optimizing many process parameters (Panda et al., 2015).

Most industries today favour heap bioleaching for extracting metals like copper, uranium, gold, and nickel from low-grade ores. This method is considered an alternative to traditional processing techniques, which include flotation, vat leaching, and reactor (Panda et al., 2012). Furthermore, heap leaching is preferred due to its faster startup times, simplicity of design, and higher quantities handled at cheap capital and operational costs (Panda et al., 2012; Pradhan et al., 2008).

According to Chowdhury & Ojumu (2014), heap bioleaching is currently an appealing approach for metal extraction from low-grade ores. Heap bioleaching is expected to be a popular method of treating low-grade chalcopyrite ores in the future (Panda et al., 2015).

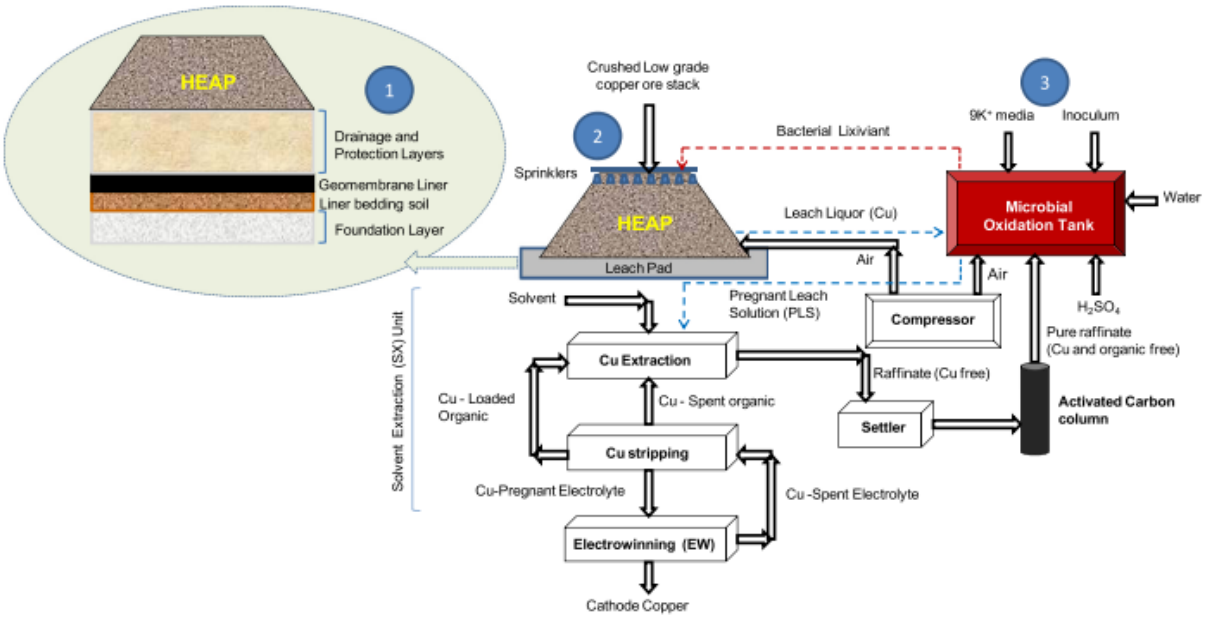

Figure 2.3: The heap bioleaching process, which includes the entire bio-hydrometallurgical process (BL-SX-EW), is specifically designed for the recovery of copper metal from low-grade chalcopyrite ores. (1) Preparing the Leach Pad and its components before loading the heap. (2) Heap loading and construction. (3) Leach pond: setting up the microbial oxidation tank. The dotted lines show how the bacterial solution and the Pregnant Leach Solution (PLS) flow by (Panda et al., 2015).

2.3.2 Tank bioleaching

To enhance gold recovery by pre-treating a sulfidic gold concentrate, in 1986 An industrial stirred-tank bioleaching plant was commissioned (Olson et al., 2003). Stirred tank processes utilize high-aeration, continuous-flow reactors arranged in series for processing minerals. An ammonia- and phosphorus-containing fertilizer is added to the first tank along with finely milled mineral concentrate or ore. An extremely aerated and temperature-controlled series of tanks carries out the mineral suspension process (Rawlings, 2005).

The fundamental limitation in the functioning of a stirred tank reactor is the amount (i.e. pulp density) of particles that can be kept in suspension. This is restricted to around 20% (w/v) of the mineral suspension. When the solids percentage in the mineral dispersion exceeds 20% (w/v), both physical mixing and microbial growth inhibition occur. For effective gas transmission, the mineral solution thickens, and the shear stress produced by the impellers in the continuous stirred tank reactor physically destroys the microbial cells (Rawlings, 2005; Chowdhury, 2012; Chukwuchendo, 2016).

Stirred-tank reactors offer a high level of efficiency in processing, although they may not always be the most cost-effective option. However, tank leaching has proven to be the most successful method for treating ore concentrates, achieving over 80% recovery of zinc from a zinc sulphide concentrate. Consequently, tank leaching is primarily used for concentrates, as low-grade ores that are not economically viable to concentrate cannot justify the processing costs. Another limitation of stirred tank reactors is their elevated construction and operational costs when compared to heap, dump, or in situ leaching methods. This factor restricts their use to high-value ores and concentrates.

Stirred-tank reactors provide an efficient level of processing, although they might not always be the most cost-effective option (Gahan et al., 2012), and tank leaching was shown to be the most successful for the treatment of ore concentrates, with more than 80% of the total zinc recovered from a zinc sulphide concentrate (Bosecker, 1997). tank leaching is only appropriate for concentrates, as low-grade ores that are not economically feasible to concentrate cannot offset the expenses of the processing (Kazadi, 2007; Mabusela, 2017). Another drawback of stirred tank reactors is their higher cost of construction and operation compared to heap, dump, or in situ leaching methods. This cost limits its use to valuable ores and concentrates (Bosecker, 1997; Rawlings, 2002).

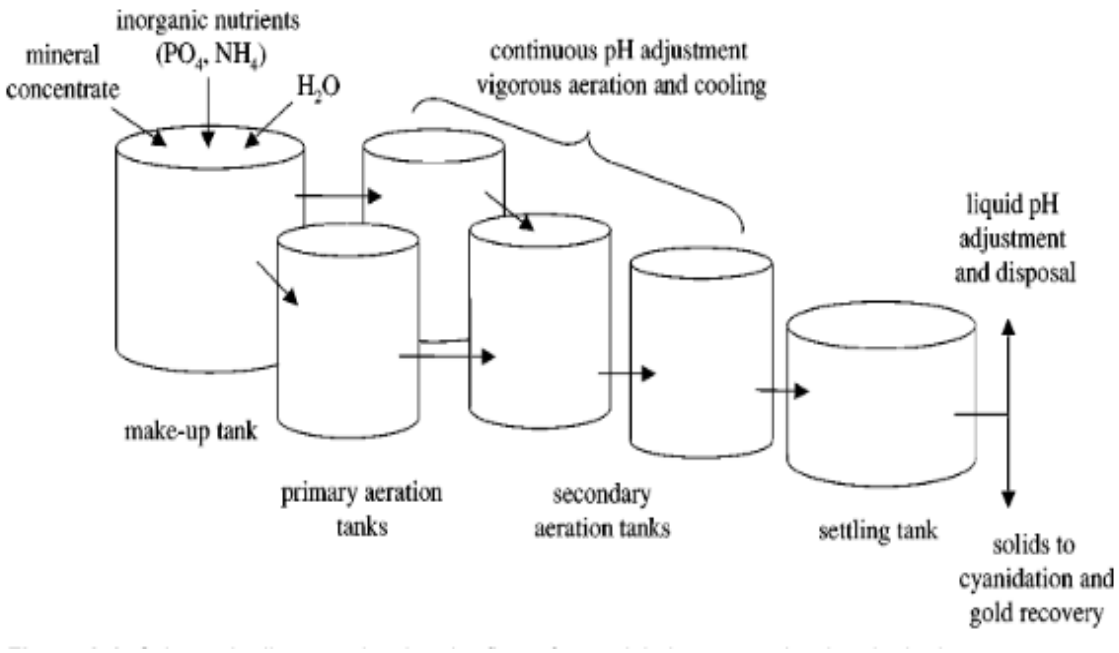

Figure 2.4: Schematic diagram showing the flow of materials between stirred tanks in the pre-treatment of gold from the arsenopyrite concentrate using the microorganisms in the stirred tank system by Wanjiya (2013).

2.4 Kinetics of microbial ferrous-iron oxidation

Leaching mechanism and nature can be better understood through kinetic studies. To gain insight and achieve the right results for plant design, to optimize the operating conditions of an existing plant, to enhance real-time automatic control, and to maximize metal recovery, kinetic studies focus on developing the most suitable kinetic model that accurately describes the process and calculates the kinetic parameters from the process (Baniasadi et al., 2019). Various kinetic models have been used to study ferrous-iron oxidation up to present, using microorganisms of different types (Ojumu et al., 2006). Different models based on empirical, Monod, and Michaelis-Menten were developed to improve the utility of metal recovery (Chukwuchendo, 2016). Many of these kinetic equations can be applied to the same experimental data since they are based on the Monod-type models, which are the basic enzymatic equations for growth rate (Chowdhury, 2012):

$$-r_{Fe^{2+}} = \frac{r_{Fe^{2+}}^{max}\,[Fe^{2+}]}{K_{Fe^{2+}} + [Fe^{2+}]} \qquad 2.8$$

Where $r_{Fe^{2+}}$ is the oxidation rate of ferrous-ions, r_{max} is the maximum rate of ferrous-ion oxidation and KS represents the substrate coefficient.

As reduced ferrous-ion is the limiting reactant, microorganisms rely on it naturally. It has been stated that success has been obtained under the ideal circumstances utilising CSTR bioreactors, although more work on optimising the kinetics has to be done (Wanjiya, 2013; Chukwuchendo, 2016). Ojumu et al. (2006) reviewed existing data to create a rate equation that was both compact and thorough, including substrate utilization, biomass synthesis, and biomass maintenance. Table 2 lists a variety of reported rate equations for ferrous-iron biooxidation.

Table 2.2: Models of kinetics published in selected journals for ferrous-ion oxidation with *At. Ferrooxidans* (Ojumu et al., 2006)

Models	Conditions
$\mu = \frac{\mu_{max}\,[Fe^{2+}]}{Y_{SX}\,K_m + [Fe^{2+}]}$	Batch STR, *T*=25-30 °C, pH= 2-2.3, Fe_T= 6 g.L^{-1}
$\mu = \frac{\mu_{max}\,[Fe^{2+}]}{K_m + [Fe^{2+}]}$	Continuous, *T*=28 °C, pH= 2.2
$\mu = \frac{\mu_{max}\,[Fe^{2+}]}{[Fe^{2+}] + K_m\left(1+\frac{[Fe^{3+}]}{K_l}\right)}$	Continuous, *T* = 30 °C, pH= 1.6, Fe_T =5-400 mM
$\mu = \frac{\mu_{max}\,([Fe^{2+}] - [Fe^{2+}]_t)}{K_m + ([Fe^{2+}] - [Fe^{2+}]_t)}$	Continuous, *T*=22 °C, Fe_T=9–22 mM, Isolate AK1
$\mu = \frac{\mu_{max}\,[Fe^{2+}]}{[Fe^{2+}] + K_S(1+K_i\,[Fe^{3+}])}$	Continuous, *T*=35 °C, pH= 1.8, Fe_T = 0.52–3.29 g.L^{-1}
$-r_{O_2} = \frac{k'_3[X][Fe^{2+}]}{[Fe^{2+}] + K_m\left[\left(1+\frac{[X]}{K'_t}+\frac{[Fe^{3+}]}{K_{tf}}+\frac{[X][Fe^{3+}]}{\alpha K'_t K_{tf}}\right)\right]}$	Initial Rate, *T*=29 °C, pH=1.8–2.0, Fe_T=0.25–26 mM
$\mu = \frac{\mu_{max}\,[Fe^{2+}]}{[Fe^{2+}] + K_S + [Fe^{3+}]\,\frac{K_S}{K_t} + \frac{([[Fe^{2+}]])^2}{K_{St}}}$	Continuous, *T*=29 °C, pH=1.8–2.0, Fe_T=2–70.8 g.L^{-1}
$-r_{Fe^{2+}} = \alpha_1\left(\frac{\rho O_2}{k_B+\rho O_2}\right)\left(\frac{[Fe^{2+}]}{[Fe^{2+}]+K_{Fe^{3+}}\left(1+\frac{[Fe^{3+}]}{K'}\right)}\right)$	Continuous, *T*=30 °C, pH=2.0, *Leptospirillum ferrooxidans*
$-r_{Fe^{2+}} = k\left(\frac{[Fe^{2+}]/[H^+]}{K_{Fe^{2+}}+[Fe^{2+}]/[H^+]+K_f[Fe^{3+}]}\right)^{0.5}\left(\frac{\rho O_2}{k_B+\rho O_2}\right)^{0.5}$	Theoretical, fitted to data from Huberts
$q_{Fe^{2+}} = \frac{q^{max}_{Fe^{2+}}}{1+K_{Fe^{2+}}\frac{[Fe^{3+}]}{[Fe^{2+}]}}$	Only fitted to *Leptospirillum* data
$\frac{d[Fe^{2+}]}{dt} = \frac{K_O e^{-\frac{Ea}{RT}}[X][Fe^{2+}]}{\left(1+\frac{[Fe^{3+}]}{K_i}\right)(K_m+[Fe^{2+}])}$	Initial Rate, *T*=30 °C, pH=2.0, Fe_T=0.45–31.5 kg.m^{-3}
$q_{O_2} = \frac{q^{max}_{O_2}}{1+\frac{K_S}{[Fe^{2+}]-[Fe^{2+}]_t}+\frac{K_S}{K_i}.\frac{[Fe^{3+}]}{[Fe^{2+}]-[Fe^{2+}]_t}}$	Continuous, *T*=30 °C, pH=1.8–1.9, FeT=0.05–0.36 M
$q_{Fe^{2+}} = \frac{K_l^* exp\left[\frac{nF}{2RT}(E^m-E_h^0)\right]\left\{1-exp\left[\frac{nF}{RT}(E^m-E)\right]\right\}}{1+\frac{K_2^*}{[Fe^{2+}]}+K_3^* exp\left[\frac{nF}{RT}(E_h-E_h^0)\right]}$	Electrochemical cell, *T*=30 °C, pH=1.8, Fe_T=0.05–1 g.L^{-1}

2.5 Bio-oxidation kinetics of ferrous-ion: Current experimental techniques

2.5.1 Microbial Growth Kinetics

Microorganisms multiply exponentially when grown in favourable settings such as optimal pH and temperature, oxygen, water, and nutrition availability. The ideal temperature range for the proliferation of iron-oxidizing microorganisms spans from 20°C to 50°C, with mesophilic and moderate thermophilic strains thriving within this range. Conversely, severe thermophilic microorganisms exhibit an optimal growth temperature exceeding 50°C. Additionally, the pH at which these microorganisms flourish is generally around 2. They are chemolithoautotrophs that feed on iron (Kazadi, 2007).

The growth equation is as follows when CN represents the concentration of cells at a given time (t):

$$\frac{\mathrm{dCN}}{\mathrm{dt}} = \mu \mathrm{C_N} \qquad 2.9$$

Determining the number of individual cells within a culture presents significant challenges, consequently, the growth of the culture is frequently quantified in terms of biomass, a parameter that is comparatively simpler to measure. Equation (2.9) becomes:

$$\frac{\mathrm{d}C_X}{\mathrm{dt}} = r_X = \mu \mathrm{C}_X \qquad 2.10$$

Upon the introduction of a seed culture into a liquid nutrient medium, the organisms exhibit a preference for the uptake of dissolved nutrients present in the medium, subsequently converting these nutrients into biomass (Shuler & Kargi, 2002). The growth process is segmented into four distinct stages: (1) lag phase, (2) exponential growth phase, (3) stationary phase, and (4) death phase (Kazadi, 2007).

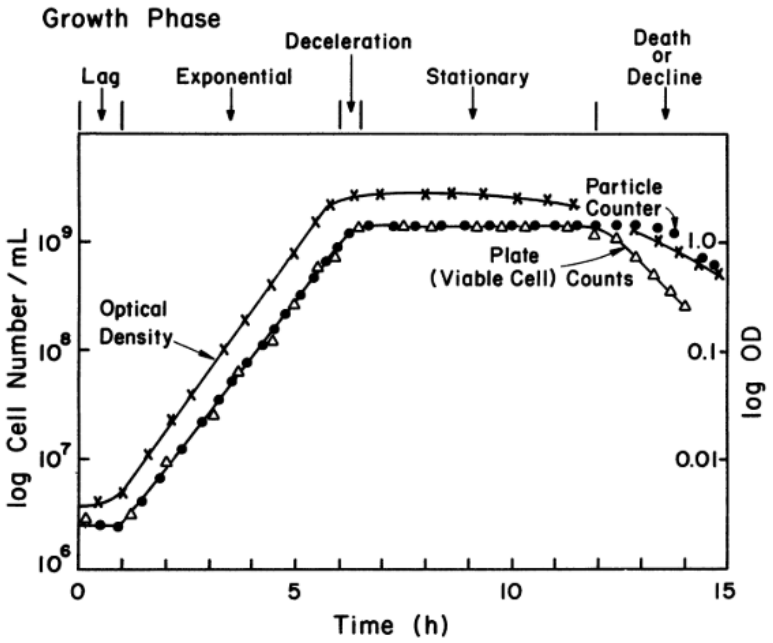

Figure 2. 5: A typical growth curve for a bacterial population (Shuler & Kargi, 2002)

2.5.1.1 Lag Phase

The lag phase commences right after inoculation and represents a period of cellular adaptation to a novel environment. Upon transfer to a new medium, microorganisms undergo a reorganization of their molecular components. The composition of the food influences the creation of new enzymes, while the production of certain enzymes may be diminished, and the cellular machinery is adjusted to suit the new environmental conditions (Shuler & Kargi, 2002). The lag phase, marked by a minimal rate of cell proliferation and the adaptation of microorganisms to their novel environment, may span from a few minutes to several hours, or even extend over the course of several days (Kazadi, 2007). The duration of this phase for a particular species of microbe is primarily influenced by the growth conditions and the characteristics of the inoculum, including its size and physiological state (Kazadi, 2007).

2.5.1.2 Exponential phase

The logarithmic growth phase is also referred to as the exponential development phase. At this stage, cells have acclimated to their new environment. Following this adaptation phase, cells may rapidly reproduce, leading to an exponential increase in cell mass and density over time. This period represents a time of balanced growth, during which all cellular components develop at an equal pace (Shuler & Kargi, 2002; Kazadi, 2007).

The rate of growth is calculated based on the gradient of the curve segment (Fig. 2.5), which reflects this stage. In this stage, the process of growth is further defined by the cell generation

time, which is quantified as the average interval between successive cell divisions across all cells within a particular culture. This is provided by (Kazadi, 2007):

$$\tau_d = \frac{ln2}{\mu} \quad 2.11$$

The growth rate of a microorganism is significantly affected by its growth conditions and type. It has been observed that when cells are in the exponential phase, they transition from a medium with limited nutrients to one with abundant nutrients. This transition leads to a brief lag phase, but the growth rate increases compared to before the transfer, a phenomenon known as a "shift up." Conversely, if cells in the exponential phase are transferred back to a medium with limited nutrients, they experience a longer lag phase. This is because the new metabolic pathways need to be activated. Consequently, a shift down in the growth rate is observed, which is slower than the rate before the transfer (Kazadi, 2007).

2.5.1.3 Stationary phase

The initiation of a stationary phase occurs when the rate of growth reaches equilibrium with the rate of death, primarily due to the depletion of nutrients, alterations in pH, and the formation of toxic metabolites, among other factors (Shuler & Kargi, 2002; Kazadi, 2007), or In the absence of cell division (zero growth rate). There may be one or more of these phenomena occurring during the stationary phase (Shuler & Kargi, 2002):

1. The total number of viable cells may decrease, but the mass concentration of cells may remain constant.
2. There is a possibility of cell lysis and a decrease in viable cell mass. Cells may grow on residues from lysed cells (cryptic growth) during a second growth phase.
3. Even though cells may not be growing, secondary metabolites are produced by their metabolism.
4. When the concentrations of specific metabolites, such as carbon, nitrogen, and phosphate, are low, cellular regulation changes. This leads to the dysregulation of metabolites, resulting in the production of secondary metabolites.

2.5.1.4 Death phase

Following the stationary phase, the process transitions into the dying phase, also referred to as the decline phase. However, it's important to note that some cell death can occur during the stationary phase, making it challenging to clearly distinguish between these two phases. During the stationary phase, cells that are no longer viable undergo lysis, resulting in the release of nutrients into the surrounding medium. These nutrients are then utilized by living organisms present in the system. The transition into the dying phase begins at the conclusion

of the stationary phase, either as a result of nutritional depletion or the buildup of toxic substances (Shuler & Kargi, 2002).

2.5.2 Batch Culture Technique

A batch culture is characterized by a microbial population that grows in a medium until the available nutrients are depleted. At this point, there is no additional food source to replenish what the bacteria have consumed, and all metabolic products remain within the culture. This accumulation of metabolites within the culture can potentially inhibit further growth (Kazadi, 2007).

Microorganisms cannot sustain growth indefinitely in a batch culture due to the absence of fresh feed and the inability to eliminate toxic by-products. The proliferation of cells halts when the availability of adequate substrates diminishes or when the concentration of toxic substances exceeds the bacterium's tolerance threshold. At this critical point, the culture may either stabilize, maintaining a balance between growth and mortality rates, or decline, with the mortality rate exceeding the growth rate (see Eq. 2.12).

Batch culture represents a dynamic process characterized by the fluctuating concentrations of substrate and biomass within the medium over time. This phenomenon is exemplified by the Biomass and Limiting Substrate Mass Balance equation:

$$\frac{dC_x}{dt} = \mu C_x - k_d C_x \qquad 2.12$$

Boon et al. (1999) explored the reaction rates of Iron-ion decomposition in single-batch systems. The preliminary phases of the research reveal a disparity in the specific growth rates (μ) as determined through off-gas analysis, in contrast to those approximated from the specific growth rate (mu batch curve) depicted in Figure 2.6, and those derived from the kinetic model (Eq. 2.14). According to Equation 2.14, the maximum acceleration of mass accumulation (ma) is anticipated to occur during the initial phase of the batch culture experiment, specifically in the presence of low $\frac{[Fe^{3+}]}{[Fe^{2+}]}$ ratios or elevated concentrations of ferrous ions. However, it is observed that the specific growth rate progressively increases until it reaches a peak, following which it remains relatively constant over a period of several hours. Boon et al. (1999), posits that the dynamic behaviour observed in growth kinetics is propelled by "significant modifications within the anabolic system," which may arise in reaction to alterations in external stimuli. Consequently, during this dynamic phase of the batch system, the rate equation for competitive product inhibition (Eq. 2.14) fails to elucidate the precise growth rate.

$$\mu = \frac{\mu_{max}\, m_o\, .Y_{ox}^{max}}{1+\frac{K_S}{[Fe^{2+}]-[Fe^{2+}]_t}+\frac{K_S}{K_i}.\frac{[Fe^{3+}]}{[Fe^{2+}]-[Fe^{2+}]_t}} - m_o\, .Y_{ox}^{max} \qquad 2.14$$

Subsequent to the dynamic phase, which is marked by periods of growth and oxidation, a swift pseudo-steady state is attained, and the trajectories depicted in Figure 2.5 align. This occurrence is confined to the concluding hours of the batch experiment, during which the ratio $\frac{[Fe^{3+}]}{[Fe^{2+}]}$ undergoes rapid changes, rendering it difficult to accurately assess its impact (Boon et al., 1999).

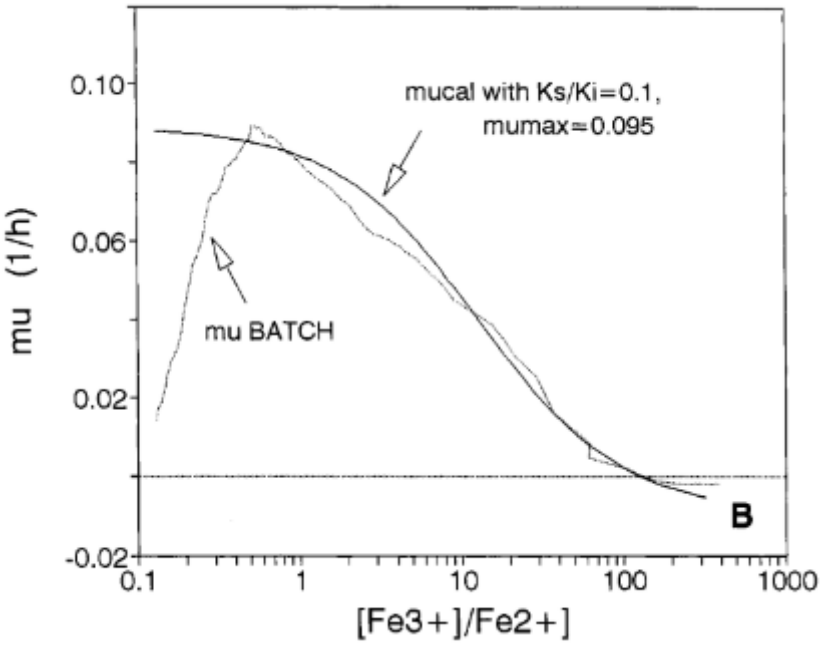

Figure 2. 6: μ versus ([Fe^{+3}]/ [Fe^{+2}]) in batch culture (Boon et al., 1999; Kazadi, 2007)

The batch culture approach has been proven to be ineffective for quantifying the influence of toxic metal ions, pH, and total iron on the steady-state kinetics of ferrous-ion bio-oxidation. The kinetic parameters, such as $qo_{2,max}$, μ_{max}, and $\frac{Ks}{Ki}$, calculated using this approach may not consistently align with those determined through continuous culture under comparable conditions (Boon et al., 1999; Kazadi, 2007).

To address these challenges, one could consider employing either a continuous method, such as a chemostat, or a fed-batch culture supplemented with a compensated substrate. However, it is unfortunate that the latter method is not appropriate for bioleaching research. This is because the feed utilized for the regeneration of ferrous ions in this process contains a chemical (reductant) that may potentially interact with bacteria (Harvey & Crundwell, 1997).

2.5.3 Continuous Culture Technique (Chemostat)

For as extended a duration as feasible, the proliferation of microorganisms within a perpetual culture is sustained during an exponential phase (Figure 2.5). This is achieved by ensuring a constant supply of fresh nutrients and the continuous removal of metabolic by-products through overflow. Upon reaching a steady state, both biomass concentrations and substrate concentrations stabilize. Consequently, the mass balance equations can be represented as follows (Kazadi, 2007):

Biomass mass balance

$$\frac{dC_x}{dt} = DC_x + \mu C_x - k_d C_x \quad 2.15$$

$$D = \mu \text{ (at steady state kd=0)} \quad 2.16$$

Substrate mass balance

$$-r_s = D(C_{Sin} - C_S) \quad 2.17$$

$$-r_s = m_S C_x + \frac{DC_x}{Y_{X/S}} \quad 2.18$$

$$D(C_{Sin} - C_S) = m_S C_x + \frac{DC_x}{Y_{X/S}} \quad 2.19$$

$$C_x = \frac{D(C_{Sin} - C_S)}{(m_S + \frac{D}{Y_{X/S}})} \quad 2.20$$

C denotes the concentration of the substrate within the feed. D represents the dilution rate, which is defined as the flow rate F divided by the volume of the continuous culture V.

Equation 2.20 shows a clear relationship between D and Cx, which means the growth of microorganisms Cx can be controlled by adjusting C's substrate concentration and dilution rate in a continuous culture (Kazadi, 2007). Continuous culture uses dilution rates to control the ratio of ferric to ferrous-ion. There is a limited range of values that can be used. Consequently, the overflow becomes equal to the feed concentration and no reaction occurs when D becomes too large (Kazadi, 2007). Therefore, D should never exceed its critical value.

Ferrous-ion bio-oxidation kinetics are most reliably studied using continuous culture as a steady-state technique. In addition to being time-consuming, this method is limited to high-

potential (Boon et al., 1999; Kazadi, 2007). The residence period (1/D) for continuous cultures generally spans from 10 to 150 hours, with steady-state assumed after three residence times.

As a result, a quicker approach for Ferrous-ion bio-oxidation kinetics research is required. Kazadi (2007), observes that the methodology, devised by Boon et al., which entails ceasing the input of a continuous culture of *Acidithiobacillus ferrooxidans* and subsequently shifting it to a batch system, is inapplicable for kinetic measurements involving *Leptospirillum ferrooxidans*. This is primarily due to the significantly brief duration of its growth cycle, which is measured in mere minutes in this particular case.

2.6 Formation of ferric-ion precipitates

Copper sulphide minerals require dissolution in the presence of an oxidizing agent, typically a ferric ion present in adequate quantities (Watling, 2006; Nazari et al., 2014). Elevated levels of ferric ions result in the precipitation of numerous compounds on the exteriors of ore particles. This phenomenon impedes the entry of leaching agents and bacterial cells onto the mineral surfaces (Córdoba et al., 2008a). In acidic conditions, both chemical and biological processes facilitate the oxidation of ferrous ions. It is noted that the biological oxidation of iron occurs at a faster rate compared to its chemical counterpart (Ozkaya et al., 2007). In the bio-leaching process, the oxidation of ferrous ions leads to the formation of ferric ions, culminating in the precipitation of various ferric-ion compounds. These compounds include schwertmannite ($Fe_8O_8(OH)_6SO_4$), ferrihydrite ($5Fe_2O_39H_2O$), and a diverse array of jarosite minerals, characterized by their chemical formulas ((K, Na, NH_4, H_2O)-$Fe_3(SO_4)_2(OH)_6$) (Gramp et al., 2008; Mabusela, 2017).

The formation of ferric ions is crucial during the microbial oxidation of ferrous ions, as they serve as a significant leaching reagent. The pH of the medium increases because the generation of ferric-ion consumes acid (Nemati et al., 1998). Furthermore, Grishin et al. (1988) and Nurmi et al. (2010) state that generally, ferric ions are very insoluble above pH 2.5 because of their high degree of hydrolysis. The pH of the liquid medium first increases when hydrogen ions are consumed. However, ferric-ion hydrolysis offsets this pH increase (Daoud & Karamanev, 2006).

$$Fe^{3+} + H_2O \longrightarrow FeOH^{2+} + H^+ \qquad 2.21$$

$$Fe^{3+} + 2H_2O \longrightarrow Fe(OH)_2^+ + H^+ \qquad 2.22$$

$$Fe^{3+} + 3H_2O \longrightarrow Fe(OH)_3 + H^+ \qquad 2.23$$

As pH plays a significant role in reactions 2.8 - 2.10, it influences both oxidation and hydrolysis (Liu et al., 2009; Mabusela, 2017). When the pH level is less than 4, ferric ions precipitate

mainly as jarosites (Fe(III) hydroxy sulphates: $AFe_3(OH)_6(SO_4)_2$, where A can be either a monovalent cation (such as Na^+, K^+, $NH4^+$ or H_3O^+)) or as an oxide and oxyhydroxide at higher pH levels (Kaksonen et al., 2014). NH_4^+ is present in high concentrations in 9K medium, which generates ammoniojarosites based on the formulation $NH_4Fe_3(SO_4)_2(OH)_6$; following the chemical equation (Daoud & Karamanev, 2006; Liu et al., 2009):

$$3Fe^{3+} + M^+ + 2HSO_4^- + 6H_2O \longrightarrow MFe_3(SO_4)_2(OH)_6 + 8H^+ \qquad 2.24$$

Ferric-ion precipitates can take numerous forms in reaction 2.11 (see Table 2.2) (Mabusela, 2017). The precipitate will take different shapes depending on the concentration of M+ in the medium solution. Taking these cations out of the medium, according to Grishin et al. (1988), may diminish the precipitation of ferric ions.

Table 3: Various forms of ferric-ion precipitates, alongside their chemical formulas, have been adapted following Mabusela, (2017) methodology

Formula	**Mineral name (precipitate)**
$KFe_3(SO_4)_2(OH)_6$	Jarosite
$NaFe_3(SO_4)_2(OH)_6$	Natrojarosite
$RbFe_3(SO_4)_2(OH)_6$	No mineral equivalent
$AgFe_3(SO_4)_2(OH)_6$	Argentojarosite
$(NH_4)Fe_3(SO_4)_2(OH)_6$	Ammoniojarosite
$TlFe_3(SO_4)_2(OH)_6$	Dorallcharite
$PbFe_6(SO_4)_4(OH)_{12}$	Plumbojarosite
$HgFe_6(SO_4)_4(OH)_{12}$	No mineral equivalent
$Pb\ (Fe,CU)_3(SO_4)_2(OH,H_2O)_6$	Beaverite
$(H_3O)Fe_3(SO_4)_2(OH)_6$	Hydronium jarosite

2.6.1 Factors affecting the formation of ferric-ion precipitate

Concentrations of ferric and ferrous ions, oxygen concentrations in cells, pH, temperature, and reactor type are all parameters that impact the rate at which *A.ferrooxidans* oxidises ferrous ions (Daoud & Karamanev, 2006). Temperature, pH, age, cation present, and dissolved carbon all play crucial roles in the precipitation of Fe^{3+} as schwertmannite or jarosites, as Liao et al. (2009) and Wang et al. (2006) points out. Furthermore, pH and temperature have a considerable impact on A. ferrooxidans' ion oxidation activities (Daoud & Karamanev, 2006). The lower pH threshold for the creation of jarosite is around pH1.5, however it varies

depending on the ionic concentration and temperature of the solution (Nurmi et al., 2010). Pourbaix diagrams may also be used to show the electrochemical stability of various iron species as a function of pH. These essential phase diagrams illustrate the pH and voltage conditions (typically within aqueous solutions) at which specific redox species maintain stability (see Figure 2.7).

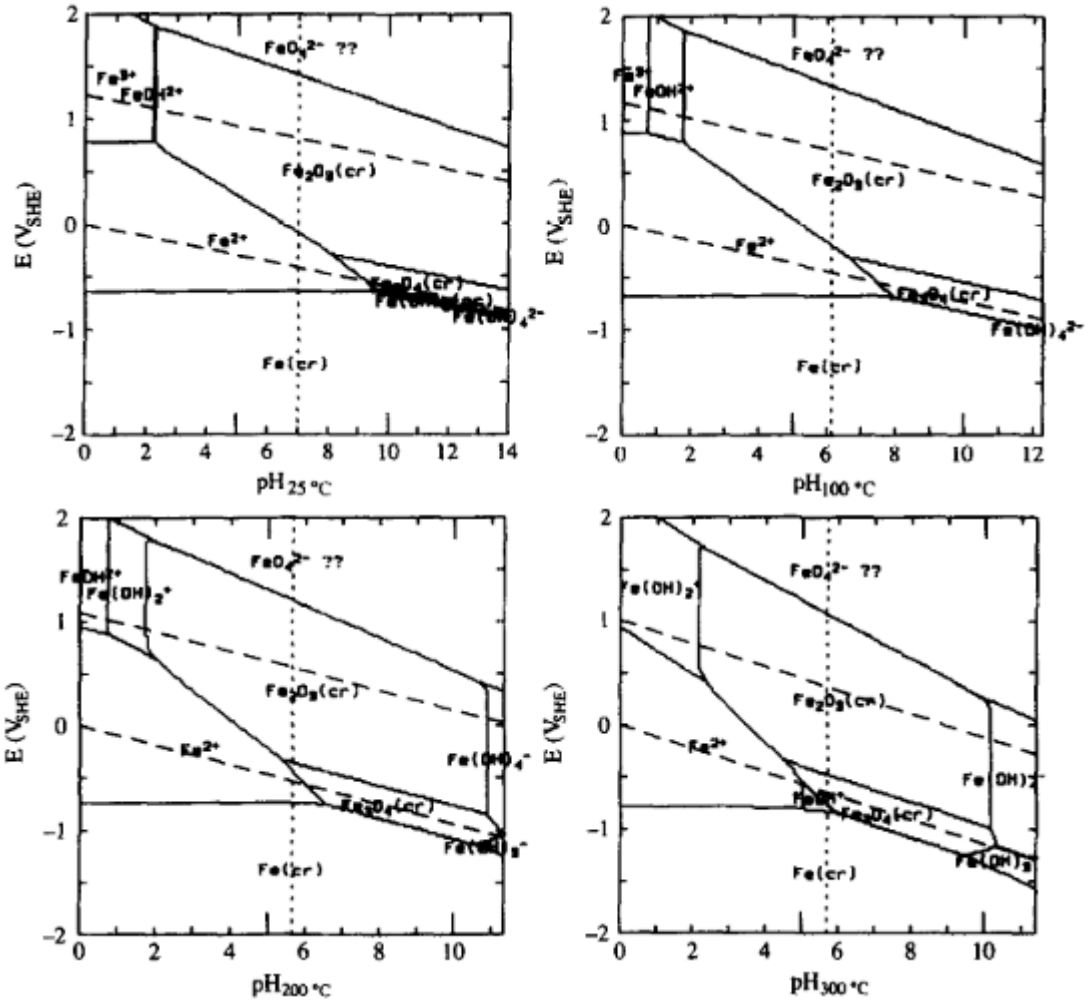

Figure 2.7: Pourbaix diagrams for iron at 10^{-6} m at 25, 100,200 and 300°C (Beverskog & Puigdomenech, 1996).

2.6.1.1 Temperature

Temperature affects ferrous-ion oxidation rates, which is an essential operational component for organisms participating in a bioleaching process. Temperature ranges for microorganisms include mesophiles (15 to 40 °C), moderate thermophiles (45 to 50 °C), thermophiles (about 65 °C), and extreme thermophiles (above 65 °C) (Chowdhury, 2012). When exposed to temperatures below their ideal operating temperature, microorganisms become dormant, and

when exposed to temperatures beyond their ideal operating temperature, they die (Chowdhury, 2012; Chukwuchendo, 2016).

A considerable amount of data demonstrates that temperature influences ferric-ion precipitation, and that as temperatures rise, ferric-ion precipitation becomes more fast and complete, and that ferric-ion precipitation rates are controlled by temperature (Mabusela, 2017).

2.6.1.2 pH

pH management is an important parameter in heap bioleaching, which involves chemolithotrophic and acidophilic bacteria (Chukwuchendo, 2016). The pH of the solution in which the ferric-ion reagent is employed has a substantial impact on the mineral sulphide leaching. High pH solution inhibits acidophilic bacteria, while ferric-ion precipitation inside heap beds can reduce permeability. However, ferric ions should not precipitate into hydroxyl and sulphate complexes to achieve successful bioleaching, which reduces the amount of ferric ions in the solution (Chowdhury, 2012).

According to Nazari et al. (2014)'s latest research, Fe^{3+} precipitates at pH levels greater than 2.2. Ojumu & Petersen (2011) conducted a study examining the impact of pH on the kinetics of Fe^{2+} oxidation by *Leptospirillum ferriphilum*. They found that the precipitation of ferric ions was significantly elevated above a pH of 1.3. Wanjiya et al. (2015) Wanjiya has reported remarkable results, demonstrating a 33% and 52% decrease in the mass of the ferric-ion precipitate following the adjustment of pH from 1.7 to 1.5 and 1.3, respectively, over a period of 10 days.

2.7 Summary and Knowledge Gaps

Ferric ions and protons are used as primary reactants in bioleaching, a chemical and microbiological process. Microorganisms are utilised largely in the microbial oxidation of ferrous ions to produce or replenish leaching agents. Bioleaching occurs in the exopolysaccharide (EPS) layer, which serves as the reaction zone. These processes include: (i) microbial oxidation of reduced Fe^{2+} to Fe^{3+}, (ii) chemical attack of sulphide minerals with Fe^{3+}, and (iii) elemental sulphur conversion to sulphuric acid.

The development of precipitates has been documented in various studies on microbial ferrous-ion oxidation and bioleaching. Chukwuchendo & Ojumu (2017) conducted research on the biooxidation and precipitation of ferrous ions under cold temperature conditions in packed column reactors. They determined the maximum rates of oxidation and precipitation. Despite the expected slow kinetics for both processes, they observed simultaneous Fe^{3+} precipitation, characterized by first-order kinetics and activation energies of 68 and 77 kJ/mol. Furthermore,

Mabusela & Ojumu (2017) explored how the initial pH of a solution affects the surface properties of Fe^{3+} precipitates. The investigation was undertaken to ascertain the correlation between operational pH and the surface charge of precipitates, in addition to their capacity for metal adsorption. The findings of their study indicated that it is possible to determine the metal adsorption capacity of a precipitate by its surface charge. Additionally, Oladipo et al. (2021) the thermodynamics, kinetics, and mechanism by which copper ions are absorbed from wastewater utilizing biogenic iron precipitate. In their examination of iron precipitates, the researchers observed a significant degree of heterogeneity in composition, expansive surface areas, and the presence of negatively charged functional groups. These characteristics augment the absorption of Cu(II) through chemisorption. Pseudo-second order model accurately described experiments, demonstrating its precision in predicting Cu(II) adsorption on biogenic iron precipitates. Furthermore, the thermodynamics parameters verified that the process is endothermic and non-spontaneous.

However, there have been few or no published investigations on the kinetics of ferric-ion precipitation. There is no information on whether the solution contains the minimum and maximum Fe^{3+} concentrations required for precipitates to develop. As a result, the goal of this study is to learn how different solution temperatures, alter the kinetics of ferric-ion precipitates as well its thermodynamic properties. This study will allow for a better understanding of the kinetics of ferric-ion precipitation, as well as an indication of how to reduce ferric-ion precipitation by adjusting solution pH and temperature, as well as a strategy for operating/designing bioleach and ferrous biooxidation processes that minimise base metal loss.

Chapter 3: Materials and Methods

This chapter provides a comprehensive overview of the materials and experimental methodology employed in the study. Additionally, it encompasses detailed elucidations of the experimental procedures and the analytical methodologies utilized throughout the research.

3.1 Materials

3.1.1 Growth medium

All experiments were conducted using analytical-grade reagents. In this study, the ferrous media contained the required amount of Fe^{2+} (12 $g.L^{-1}$) added as $FeSO_4.7H_2O$, 21.96 $(NH_4)_2SO_4$, 6.36 $(NH_4)_2HPO_4$, 13.32 K_2SO_4, and 120 mL of Vishniac solution (Vishniac & Santer, 1957), adjusted to the desired pH with concentrated H_2SO_4 to reach the target pH 0.7 ≤ pH ≤ 1.30 (Ojumu et al., 2009; Chukwuchendo, 2016). To prepare the Vishniac solution, an

EDTA solution of 15 $g.L^{-1}$ ($C_{10}H_{14}N_2Na_2O_8.2H_2O$, M = 372.24 $g.mol^{-1}$) was prepared by dissolving it in 200 mL of 6% (w/v) KOH (Mabusela, 2017). The following chemicals were added to 400 mL dH2O separately: 1.1 g $(NH_4)6Mo_7O_{24}.4H_2O$, 9.24 g $CaCl_2.2H_2O$, 1.62 g $CoCl_2.6H_2O$, 5.06 g $MnCl_2.4H_2O$, 22 g $ZnSO_4.7H_2O$, 1.58 g $CuSO_4.5H_2O$, 5.0 g $FeSO_4.7H_2O$. All components were required to undergo comprehensive dissolution prior to the addition of the EDTA and Vishniac solutions, with the resultant volume being increased to one litre through the use of sterile distilled water. To mitigate the risk of ferrous ion oxidation, the solution was maintained at a refrigerated temperature (Mabusela, 2017).

3.1.2 Bacteria culture

From the University of Cape Town's Centre for Bioprocess Engineering Research (CeBER), a selection of microorganisms was procured. These microorganisms were cultivated on pyrite concentrate within a 1 L batch continuously stirred tank reactor, maintained at a temperature of 37 °C, and subjected to agitation at a rate of 450 rpm. To ensure the sustained activity of the microorganisms, a subculturing process was implemented on a weekly basis. This process involved the removal of approximately 100 mL of the slurry, followed by the refilling of the volume to the litre mark with fresh media. Additionally, 2.5 grams of fresh pyrite concentrate were added to the mixture.

3.2 Methods

3.2.1 Experimental study on the effect of operating temperature

Experiments involving batch culture were conducted in 250 mL shakeflasks, which were placed within a shaking incubator. To ensure a constant pH of 1.7 was maintained within the solution medium, concentrated H_2SO_4 was utilized. The temperature was adjusted to 30, 35, and 40 degrees Celsius over the course of the experiment, with the solution being agitated at a rate of 120 revolutions per minute. Throughout the 14-day incubation period, various parameters were measured daily, including redox potential, total iron content, pH, and ferrous ion concentration.

3.3 Analytical procedure

3.3.1 Iron determination

For the purpose of mass balance, daily samples were systematically collected and quantified. The redox potentials of these samples were measured within the bioreactor employing redox electrodes made of silver (Ag)/silver chloride (AgCl). Before any measurements, the redox probe underwent regular calibrations under conditions that closely resembled those within the

bioreactor. As a consequence of adopting this methodology, it was possible to ascertain the ratio between ferric and ferrous ions within the bioreactor solution (refer to section 3.3.2). Titrations employing potassium dichromate, in conjunction with the BDS indicator, were performed to ascertain the total iron concentration within bioreactor solutions (Mabusela, 2017). Accordingly, the total iron concentration [Fe^{tot}] and redox potential [Eh] values were calculated during the experiment to determine ferric and ferrous ion concentrations, respectively:

$$[Fe_T] = [Fe^{3+}] + [Fe^{2+}] \quad 3.1$$

In the context of [Fe_T], "[Fe_T]" represents the total iron concentration (mmol Fe^{2+} L^{-1} h^{-1}). Conversely, "[Fe^{3+}]" denotes the concentration of ferric ions (mmol Fe^{3+} L^{-1} h^{-1}). Lastly, "[Fe^{2+}]" signifies the concentration of ferrous ions (mmol Fe^{3+} L^{-1} h^{-1}).

3.3.2 pH and redox potential measurements

The redox potential and pH were quantified employing a CRISON GLP 21 pH/Eh meter instrument. Prior to each measurement, the pH electrodes underwent calibration at pH values of 4, 7, and 9 using Merck's buffer solutions.

As the sole redox couple present within the bioreactors, the redox electrode, specifically the Ag/AgCl electrode, underwent calibration in accordance with the half-reaction representing the oxidation of ferrous ions to ferric ions ($Fe^{2+} \rightarrow Fe^{3+} + e$). The process of plotting the calibration curve was illustrated in Equation 3.2, utilizing the Nernst equation under the experimental conditions. This calibration allowed for the determination of the ratio [Fe^{3+}]/[Fe^{2+}].

$$E_h = E'_h + \frac{RT}{nF} ln \frac{[Fe^{3+}]}{[Fe^{2+}]} \quad 3.2$$

In the given equation, Eh denotes the standard reduction potential, while [Fe^{3+}]/[Fe^{2+}] signifies the ratio (R) between the concentrations of ferric and ferrous ions. In solutions where the concentrations of ferric and ferrous ions are equal, the potential, denoted as E′h, encompasses the potential of the solution that takes into consideration the activity coefficients, complex formation, the type of electrode, and the issue of electrode fouling. An E′h value can be obtained from the intercept between Eh and ln ([Fe^{3+}]/[Fe^{2+}]), while the slope is used to obtain RT/nF (Mabusela, 2017).

3.4 Analysis of kinetic data

3.4.1 Kinetic equation of microbial ferrous-ion oxidation

The Arrhenius equation can be employed to delineate the maximum microbial utilization rate of ferrous iron ($r_{Fe^{2+}}^{max}$), and subsequently, this value can be expressed in terms of Equations 3.3 and 3.4

:

$$r_{Fe^{2+}}^{max} = K_0 exp\left(-\frac{E_a}{RT}\right) \quad 3.3$$

$$lnr_{Fe^{2+}}^{max} = -\frac{E_a}{R}\left(\frac{1}{T}\right) + lnK_0 \quad 3.4$$

The plot of the maximum $lnr_{Fe^{2+}}^{max}$ versus 1/T can be utilized to determine the activation energy (Ea) and the frequency factor (K_0) for microbial ferrous-iron oxidation kinetics. From the plot, it is possible to calculate the activation energy (Ea) and the pre-exponential factor (K_0) by drawing a straight line with a slope of -Ea/R and an intercept of lnK_0. The value of R is the gas constant, which is 8.314 J mol^{-1} K^{-1}. After plotting the experimental data, a trend-line must be inserted, and the correlation coefficient (R^2) value determined to investigate the accuracy of the experimental data obtained. A correlation coefficient value above 0.90 was considered to be sufficient for the correlation of experimental data and mathematical models.

3.4.2 Estimation of activation energy

The activation energy facilitates the determination of the energetic barrier that metal ions are required to surmount in order to commence a process. In Equation 3.5, the linearized version of the Arrhenius equation is used to calculate this energy:

$$\ln k = \frac{Ea}{R}\,\frac{1}{T} + \ln A \quad 3.5$$

The term Ea (kJ/mol) signifies the activation energy, whereas k represents the equilibrium rate constant. The constant A is the Arrhenius constant, with R (8.314 J/mol K) serving as the gas constant, and T (K) denotes the absolute temperature of the solution. The gradient of the graph, derived from the equation for ln(k)/1/T, as outlined in Equation 3.7, can be employed to determine the value of Ea.

3.5 Determination of thermodynamic properties

The evaluation of thermodynamic parameters is crucial to determining a system's feasibility and mechanism. Eyring-Polanyi's equation can be used to approximate thermodynamic

parameters particularly enthalpy change (∆H), free energy change (∆G), and entropy change (∆S) (Encinar et al., 2016; Zhou et al., 2018; Oladipo, 2022).

From the Eyring-Polanyi equation to calculate Gibbs free energy, ΔG can be written as:

$$k = k\frac{k_B T}{h}\exp\left(-\frac{\Delta G}{RT}\right) \quad 3.6$$

Taking the natural logarithm and substituting, where:

$$\Delta G = \Delta H - T\Delta S \quad 3.7$$

ΔH and ΔS are enthalpy and entropy of the activation energy respectively, and can be written as:

$$\ln\frac{k}{T} = -\frac{-\Delta H}{R}\left(\frac{1}{T}\right) + \left[lnk + \ln\left(\frac{k_B}{h}\right) + \frac{\Delta S}{R}\right] \quad 3.8$$

Where k is the transmission coefficient with a value of one, k_B is the Boltzmann constant ($1.38\text{x}10^{-23}$ J/K), and h is Planck's constant with a value of ($6.63\text{x}10^{-34}$ J.s).

By constructing a linear regression model utilizing the natural logarithm of the ratio of k over temperature to the reciprocal of temperature, and then applying the intercept and slope values, it is possible to approximate the values of ∆S and ∆H.

3.6 Characterisation of ferric ion precipitate

In-depth analyses of both chemical and microstructural characteristics were performed on the precipitates collected at the conclusion of each experimental phase, aiming to elucidate their inherent nature. These analyses encompassed thermogravimetry analysis (TGA), scanning electron microscopy (SEM), Fourier transform infrared spectroscopy (FTIR), and X-ray diffraction (XRD). Characterising these precipitates is crucial for comprehending their behaviour, properties, and potential applications.

3.6.1 X-ray diffraction (XRD)

To provide chemical insights into the composition of the precipitate samples under investigation, XRD analysis was employed to examine the crystal structure and identify the crystalline phases present. The process of identifying phases was examined using an X-ray diffractometer, specifically the Bruker D2 Phaser model, which was outfitted with a Cu-Kα radiation source (wavelength, λ = 1.5406 Å) and a scintillation detector. The device was run at a current of 10 mA, a step size of 0.02°, a tube voltage of 30 kV, a scan speed of 0.5 s per step, and a scan range of 2θ from 5 to 90°.

The crystallite size of the iron precipitate, identified as the smallest and most probable to exist in a single-crystal powder form, was ascertained through the process of X-ray diffraction broadening. This calculation was executed employing Scherrer's equation, as outlined below (Holzwarth & Gibson, 2011):

$$d = \frac{k\lambda}{\beta cos\theta} \quad 3.9$$

In this particular scenario, 'd' denotes the crystallite size, measured in nanometers, perpendicular to the lattice planes. 'k' represents the crystallite-shape factor, which is set at 0.9. 'λ' signifies the wavelength of the X-rays, with a value of 0.15406 nm. 'β' denotes the width of the X-ray diffraction peak, measured in radians, and 'θ' represents the Bragg angle, also measured in radians.

3.6.2 Scanning electron microscopy (SEM)

The morphology and surface characteristics of the solid particles present in the samples were carefully examined under an electron microscope. This analysis was conducted utilizing a scanning electron microscopy (SEM) instrument, the JCM-7000 NeoScope™. This microscope was furnished with secondary electron (SE) and backscattered electron (BSE) detectors. The instrument was set to a landing voltage of 5 kV with the secondary electron detector activated, and imaging was performed at a magnification of 100X.

3.6.3 Fourier Transform Infrared Spectroscopy (FTIR)

FTIR was utilised for both detailed and quantitative assessments of solid samples, aiding in the identification of the various types of chemical bonds present. The samples were quantified with a Fourier transform infrared spectrometer (Perkin Elmer UATR Two). Data was collected within the wavelength spectrum spanning from 4000 to 400 cm^{-1}, achieving a resolution of 4 cm^{-1}.

3.6.4 Thermogravimetry analysis (TGA)

The Thermogravimetry analysis (TGA) was employed for the assessment of the thermal stability of precipitate samples, through the determination of the percentage weight loss at distinct stages of sample disintegration. This analysis was carried out using the instrument (NETZSCH STA 449 F5 Jupiter®), which is equipped with a furnace designed to measure mass changes under temperature influence. A quantity of approximately 20 mg of the powdered sample was subjected to heating within an aluminium crucible pan, commencing from an ambient temperature and progressing to a final temperature of 1000 °C, at a heating rate of 20 °C per minute. This procedure was executed within a nitrogen-enriched

environment, which functioned simultaneously as both a reactive and protective gas medium, characterized by flow rates of 50 mL/min and 20 mL/min, respectively.

Chapter 4: Kinetics and Thermodynamics of Iron Precipitation During Microbial Ferrous-ion Oxidation

4.1 Introduction

The comprehension of the kinetics involved in the precipitation of ferric ions during microbial oxidation is of paramount importance across a range of disciplines, such as environmental engineering, geochemistry, nuclear reactor technology, and microbiology. Microorganisms significantly contribute to the process of iron oxidation, leading to the formation of ferric-ion precipitates, which can have important implications for processes such as acid mine drainage formation and metal leaching (Brock & Gustafson, 1976).

There is extensive literature showing that iron precipitation occurs during hydrometallurgical and biohydrometallurgical treatment of sulphide minerals, and this occurrence is inevitable (Oladipo, 2022). Moreover, the formation of precipitates acts as a pathway for the removal of unwanted alkali ions, iron, or sulfate ions from the processing circuit (Oladipo et al., 2021). Although the rate of precipitate formation can be reduced, substantial buildup over extended periods of operation can result in slow reactions and decrease the effectiveness of the bioleaching process by occluding desired metals inside precipitate residues (van Hille et al., 2010; Wu et al., 2016; Oladipo et al., 2021).

The kinetics of ferric-ion precipitation have received little attention. Consequently, this research investigates the rate of ferric ion precipitation in a typical ferrous-ion biooxidation system. A better understanding of ferric-ion precipitation kinetics will help promote a possible strategy for operating/designing bioleaching and ferrous biooxidation processes, to minimise base metal loss.

4.2 Methodology

The study aimed to quantify the precipitation of iron in shake flasks, conducted at temperatures of 30, 35, and 40 °C, and a pH of 1.7, with a solution containing a total concentration iron of 12 g/L. Additionally, the kinetics and thermodynamics of the process were explored in this section. This study was designed and carried out as described in Sections 3.3, 3.4, and 3.5.

4.3 Results and Discussion

4.3.1 Variations in the redox potential with time

Figure 4.1 depicts the evolution of redox potential over a temperature range from 30°C to 40°C. The process of oxidation involving ferrous ions by microorganisms can be regarded as the direct cause of changes in redox potential during bio-oxidation (Third et al., 2000; Oladipo,

2022). Given that increased redox potential leads to increased ferrous oxidation (Mabusela, 2017) higher oxidation rates and ferric-ion production rates were observed at temperature 40°C. According to Seitkamal et al. (2020), at lower temperatures, the rates of oxidation significantly decrease, likely due to both reduced microbial activity and slower chemical reaction rates. Therefore, the delayed increase in redox potential at 30 and 35 °C signifies the slow metabolic activity of *Leptospirillum ferriphilum* during the lag phase, leading to the slow rate of oxidation of ferrous ions. As can be observed, maximum oxidation was obtained in less than 78 hours. This occurs because Fe^{3+}/Fe^{2+} solutions tend to achieve a chemical balance where the actions of both Fe^{3+} and Fe^{2+} ions are equal (Córdoba et al., 2008b). Throughout the duration of the experiment, the ferrous ions underwent rapid oxidation, resulting in an elevated redox potential that surpassed 638 mV and remained there throughout.

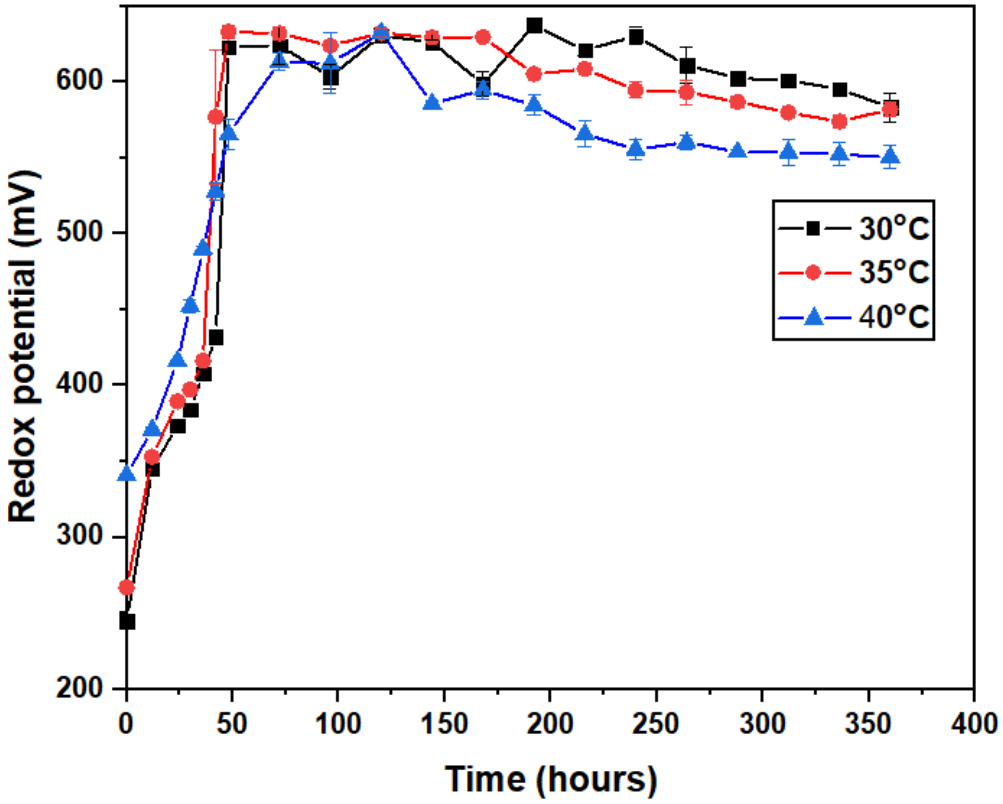

Figure 4.1: Changes in redox potential over time at different temperatures

4.3.2 Variations in the pH values with time

Figure 4.2 depicts how the initial solution pH values vary over time. The overall pattern discernible in the Figure is characterized by an initial elevation in solution pH, subsequently followed by a notable decrease in pH. Conversely, the reduction in pH is attributed to the precipitation of ferric ions, which is subsequently followed by the liberation of hydronium ions.

Conversely, the elevation in pH is attributed to the utilization of hydronium ions during the oxidation of ferrous ions (Mabusela, 2017; Oladipo, 2022). Moreover, a variation in the pH of a solution can be linked to the oxidation of ferrous ions, which is the single reaction responsible for the change (Qiu et al., 2005; Mabusela, 2017). At 35°C in the 48th hour, pH dropped sharply, probably due to a high concentration of precipitated iron. The steady increase in pH at a temperature of 40°C can be attributed to the diminished activity of microorganisms in acidic conditions. This is due to the necessity of a considerable quantity of ferric ions to reduce the pH of the solution (Jin et al., 2013), it can be confirmed that at the observed pH levels, almost all the ferrous-ion had been oxidized by the 48th hour, resulting in the solution being predominantly filled with ferric ion.

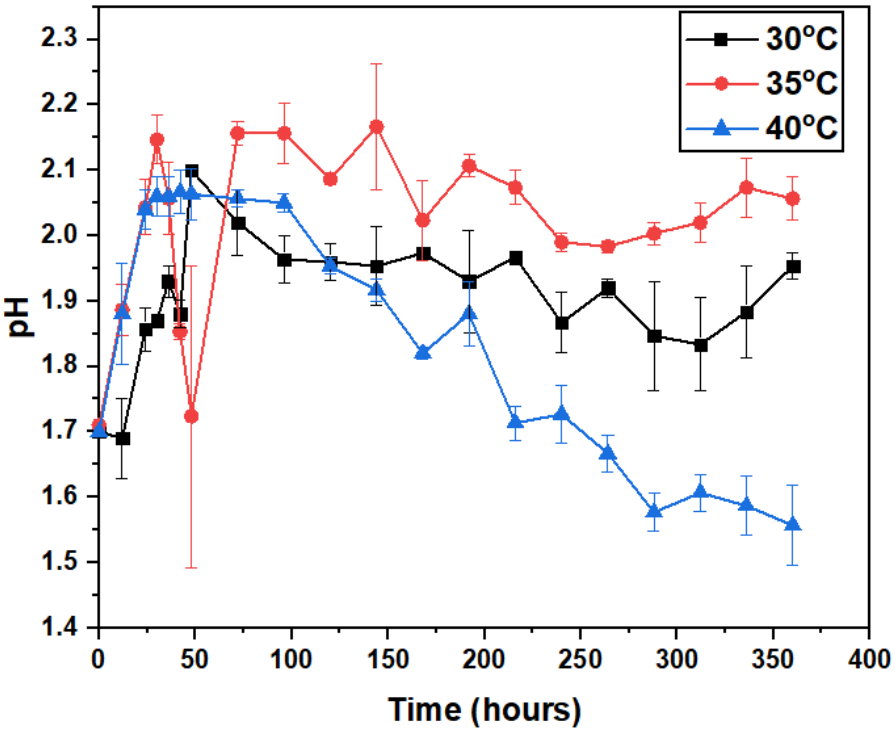

Figure 4.2: Changes in initial pH over time

4.3.3 Effect of temperature on the amount of iron precipitate

The mass of the iron precipitates produced over the 14-day duration of the process is shown in Figure 4.3a. As the temperature rises, there is an increase in the quantity of iron precipitate formed. The trend was also observed by Dopson et al. (2007); however, their study was conducted over a temperature range of 2 – 40 °C. A pH of 1.7 was used for all the temperatures

investigated in this study. The iron precipitate was lowest at 30°C (0.22 g), followed by 0.62 g at 35°C, and finally, the biggest amount was observed at 40 °C (2.48 g).

Figures 4.1 and 4.2 can also provide a good explanation for the results in Figure 4.3. The substantial formation of iron precipitate at the investigated temperatures is in line with the high redox potentials, which fall within the critical range essential for substantial precipitation (Córdoba et al., 2008b). Hence, the amount of iron that precipitates is directly proportional to the length of time permitted for a solution medium abundant in ferric ions to undergo the process, as long as the redox potential stays within the critical range (Mabusela, 2017; Oladipo, 2022). The decrease of pH resulting from the precipitation of ferric ions as bio-oxidation progresses is illustrated in Figure 4.2. According to Figures 4.2 and 4.3a, The extent of the pH gradient diminishes in direct relation to the quantity of iron precipitated. Additionally, Figure 4.3 a) and b) illustrate that a substantial amount of precipitates commenced their formation approximately 24 hours into the process, during which time the concentration of ferric ions reached its maximum (1.22 g/L ± 0.05 at 30 ºC, 1.25 ± 0.03 at 35 ºC, and 1.2 ± 0.05 at 40ºC). The maximum concentrations are observed to occur at approximately similar times and values, with no significant discrepancies. This indicates that temperature did not exert a substantial influence on the maximum threshold concentration necessary for the formation of ferric ion precipitates. Consequently, an average concentration of 1.22 g/L of ferric ion precipitates is deemed essential for precipitation to occur. Moreover, as the concentration of ferric ions decreased within the system (Figure 4.3b), a corresponding increase in the mass of precipitates was observed (Figure 4.3a), attributed to the loss of ions during the precipitation formation. The generation of precipitates continued throughout the duration of the operational process.

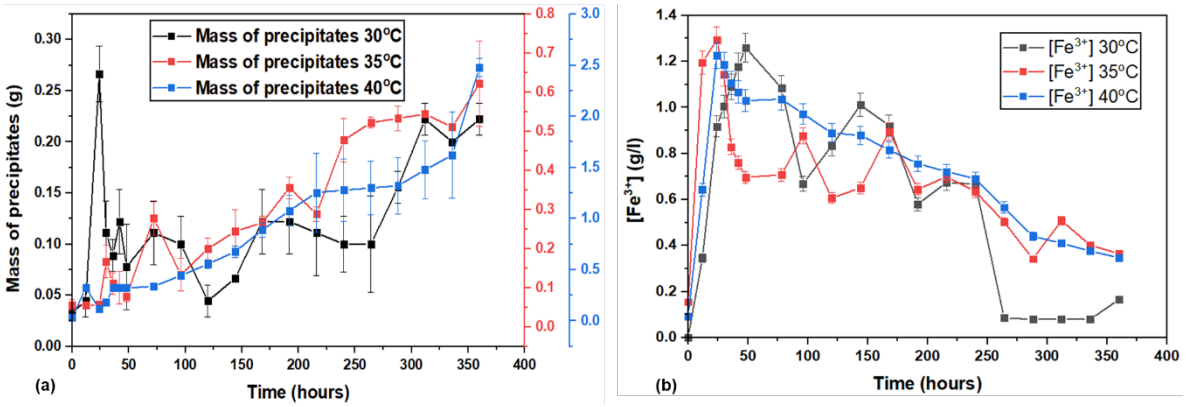

Figure 4.3: a) Mass of ferric-ion precipitate generated during operation; b) Ferric-ion concentrations obtained at different temperatures

The mass of the iron precipitate identified in this research is found to be analogous to that observed in prior studies. A plausible explanation could be the difference in strain applied

(Coram & Rawlings, 2002) and the type of reactor utilized (Daoud & Karamanev, 2006). The strain type has a significant impact on the development of ferric ion precipitate, far more than previously believed (Mabusela, 2017). In a recent study, Oladipo (2022) conducted an investigation into the influence of the initial pH of the solution on the precipitation of iron during the biooxidation of ferrous ions. The obtained mass of iron precipitates after 14 days was 11.49 g compared to 2.48 g in this study. The differences between the two studies arise from the high pH of the solution and the large reactor used in that experiment.

However, the total mass of 2.48 g of precipitate at a pH of 1.7 in this research is significantly greater than what Daoud & Karamanev (2006) the experiment yielded, which was only 0.17 g. Although their experiment was carried out in a smaller reactor similar to this study; the elucidation for this disparity lies in the fact that the *A. ferrooxidans* employed by the investigators demonstrated reduced efficacy as a biocatalyst in comparison to *L. ferriphilum*, the species utilized in the present study. This phenomenon can be attributed to the fact that *L. ferriphilum* exhibits a more robust affinity for ferrous ions and possesses a greater capacity to endure elevated concentrations of ferric ions (Petersen & Ojumu, 2007). In environments with elevated levels of oxidation, as indicated by high redox potentials, *Leptospirillum spp.* have been shown to exhibit a markedly greater capacity for iron oxidation compared to *Acidithiobacillus ferrooxidans* (Oladipo, 2022). Another significant factor to consider is the pH and temperature of the environment in which the process occurs. *L. ferriphilum* exhibits a greater tolerance to low pH levels and higher temperatures compared to *A. ferrooxidans*. (Rawlings, 2002; Rawlings, 2005).

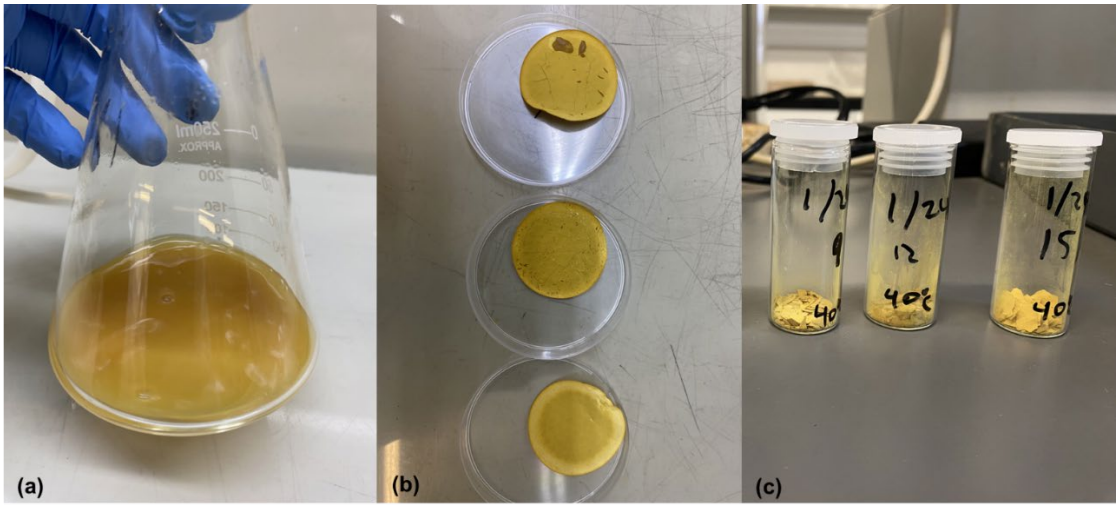

Figure 4.4: (a) Iron precipitate in solution, (b) sample of the iron precipitates formed following the filtration and drying processes on filter paper, and (c) dried iron precipitates

Table 4.1: Comparative analysis of literature studies in relation to precipitate formation during ferrous-ion bio-oxidation

Bacteria employed	**Reactor type, working volume**	**Experimental conditions**	**Precipitate amount**	**References**
Thiobacillus ferrooxidans	Packed-bed reactor, 50 mL	23°C, pH 1.35	0.24 g after 1 month	Grishin et al. (1988)
Acidithiobacillus ferrooxidans	Erlenmeyer flask, 250 mL	260 rpm, 35°C, pH 2.0	0.17 g after 46 h	Daoud & Karamanev (2006)
Acidithiobacillus ferrooxidans	Erlenmeyer flask, 500 mL	180 rpm, 30°C, pH 2.0	2.64 g after 46 h	Liu et al. (2007)
Thiobacillus ferrooxidans	Erlenmeyer flask, 250 mL	110 rpm, 28 °C, pH 1.99	~13.00 g after 7 days	Liu et al. (2009)
Acidithiobacillus ferrooxidans	Packed-column bioreactor, 500 mL	38.6°C, aeration rate 20 mL/s, dilution rate 0.05 h^{-1}, pH 1.7	7.08 g after 10 days	Wanjiya (2013)
Leptospirillum ferriphilum	Continuous stirred tank reactor, 1 L	350 – 400 rpm, 35°C, pH 2.0, aeration rate 3 mL/s	13.26 g after 14 days	Mabusela (2017)
Leptospirillum ferriphilum	Continuous stirred tank reactor, 1 L	550 rpm, 35°C, pH 2.2, aeration rate 3 mL/s	11.49 g after 14 days	Oladipo (2022)
Leptospirillum ferriphilum	Erlenmeyer flask, 250 mL	120 rpm, 40°C, pH 1.7	2.48 g after 14 days	This study

4.3.4 The rate of ferric-ion precipitation and activation energy

The experimental data in this research were delineated through the application of first-order differential equations concerning ferric-ion. As noted by (Chukwuchendo, 2016), in the process of determining the rate constants for ferric precipitates, it was observed that the first-order rate equations could be used to determine rate constants. Hence, the findings in this study, as presented in Figure 4.5 illustrate a rise in the concentration of ferric ion precipitation over time, which is directly proportional to the concentration increase observed during this interval until the maximum threshold of ferric ions in the solution is attained (refer to Figure

4.3b). Furthermore, Table 4.2 indicates that the rate constants demonstrate an upward trend with increasing temperatures throughout the examination of the ferric precipitate.

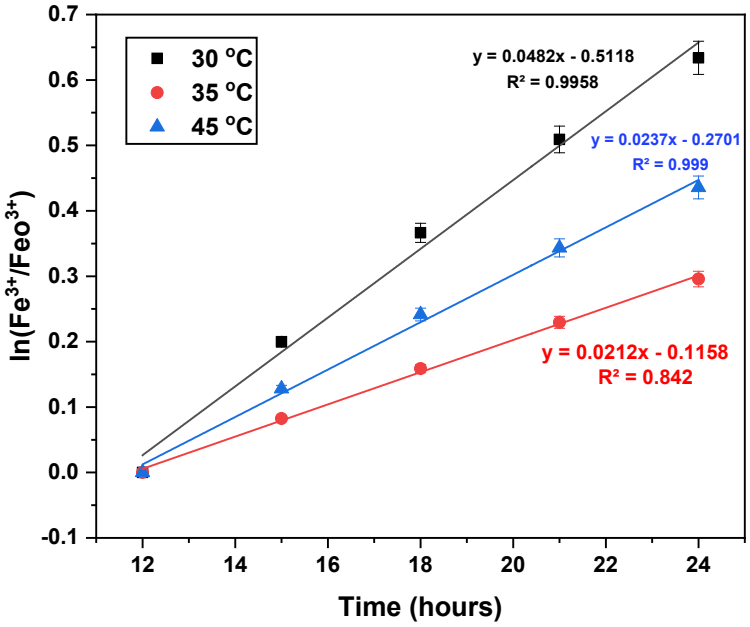

Figure 4.5: The first-order plot of the kinetics of ferric ion precipitate.

Table 4.2: First-order rate constants of ferric-ion precipitate

Temperature (°C)	1st order (k_1) (h^{-1})	R^2 (k_1)
30	0.5118	0.9958
35	0.2701	0.999
40	0.1158	0.842

The influence of temperature on the synthesis of ferric precipitate can be further understood through the application of the Arrhenius Equation (3.7). This equation was employed to ascertain the activation energy (Ea) across the temperature spectrum under investigation. This was achieved through the graphical representation of the natural logarithm of the rate constant (Ln k) versus temperature (1/T), yielding a linear relationship (see Figure 4.5). From this graph, The values for activation energy (117.2 kJ/mol) and the frequency factor (K) with the value of 2.94 X 10^{20} were determined. The slope of the Arrhenius plot was employed to determine the activation energy of the ferric precipitate, utilizing the experimental data collected within the temperature interval of 30 to 40°C. This was accomplished by utilizing a

first-order differential equation. The positive value of the activation energy suggests that an elevation in temperature enhances the formation of ferric precipitates. Additionally, this process is endothermic in nature.

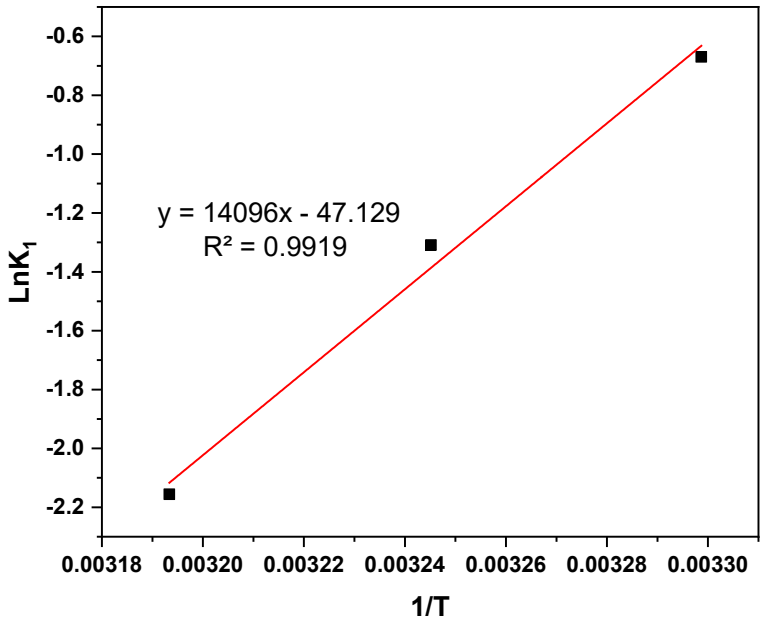

Figure 4.6: The Arrhenius plot of the effect of temperature on ferric-ion precipitate formation

4.3.5 Thermodynamic properties

The intercept and slope of a linear Arrhenius-Eyring-Polanyi plot of ln K/T vs 1/T were used to determine enthalpy change (ΔH) and entropy change (ΔS), respectively (Figure 4.5). Table 4.3 presents a summary of the obtained thermodynamic properties (ΔH, ΔS, and ΔG).

From the obtained thermodynamic properties (Table 4.3), the positive enthalpy change (ΔH) indicates that the precipitation process occurring at the examined temperatures is characterized by an endothermic nature. Furthermore, the positive entropy of solution (ΔS) value signifies an increase in dissociation and randomness throughout the reaction. This, in turn, suggests that the reaction is energetically favourable, thereby facilitating the spontaneity of the chemical reaction. As observed in this study, the positive ΔG values indicate that the formation of precipitates is non-spontaneous, and necessitates the input of energy and agitation. According to Hofer & Steininger (2023) the spontaneity of a reaction is contingent upon the sign similarity between the ΔS and ΔH. The nature of the reaction, whether it is endothermic or not, influences its spontaneity, with reactions characterized by $\Delta S > 0$ being more likely to be spontaneous, particularly at high temperatures. Therefore, given that the findings indicate that the process of precipitate formation is non-spontaneous, and it necessitates a significant amount of energy to facilitate its progression.

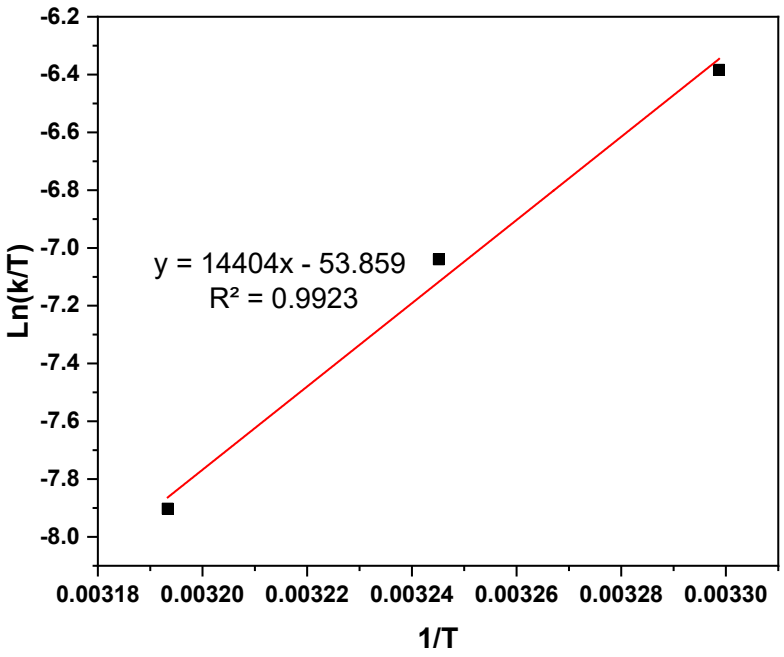

Figure 4.7: Arrhenius-Eyring-Polanyi plot for determination of Gibb's free energy.

Table 4.3: Thermodynamic properties of iron precipitate formation

Temperature (°C)	ΔH (kJmol^{-1})	ΔS (kJmol^{-1}K^{-1})	ΔG (kJ)
30	120	0.25	43.89
35			42.64
40			41.39

4.3.6 Conclusion

The research explored the quantification, kinetics, and thermodynamic properties of ferric ion precipitates under constant pH conditions and varying temperatures. The highest oxidation and precipitate production rates were obtained at the highest temperature (40 °C) investigated in this study, which was due to the high metabolize of microorganisms. A significant amount of precipitates started forming after 24 h at an average [Fe^{3+}] threshold of 1.22 g/L. The reaction kinetics followed the first-order pathway with the activation energy for the precipitate formation determined to be 117.2 kJ/mol. The positive values of the estimated thermodynamic parameters (ΔH, ΔS, and ΔG) suggest that the process is chemically favoured, endothermic and non-spontaneous, respectively. Since the results show that the process of precipitate formation is non-spontaneous, it thus requires high energy for it to proceed.

Chapter 5: Surface properties of generated iron precipitates during microbial ion oxidation

5.1 Introduction

Extensive research within the scholarly literature has conclusively shown that the precipitation of iron during the dissolution of sulphide minerals is an unavoidable consequence of both hydro- and bio-hydrometallurgical processes (Qiu et al., 2005; Nurmi et al., 2010). Nevertheless, in the context of bioleaching operations, the precipitation of ferric ions is considered undesirable due to its adverse effects (Daoud & Karamanev, 2006; Mabusela, 2017). Although the formation of precipitates can be somewhat mitigated, the buildup of these precipitates over extended periods of operation can lead to reduced reaction rates and diminish the efficiency of bioleaching processes by causing the targeted metals to become encapsulated within the precipitate residue (Nurmi et al., 2010; Oladipo et al., 2021).

The characterization of potassium jarosite during biooxidation is a multifaceted process, influenced by a variety of factors, with the temperature being a particularly influential element. Research has demonstrated that elevated temperatures can result in a greater conversion to jarosite-group minerals (Sowers et al., 2023). Moreover, Eftekhari et al. (2020), has indicated that the morphology and particle size of jarosite can be markedly altered by variables including temperature, pH, and agitation speed throughout the crystallization process. Hence, this chapter delineates the characterization outcomes for the synthesized ferric-ion precipitates that were produced during the microbial oxidation of ferrous ions in shake flasks, with a view to understanding its behaviour during biooxidation processes, as it can influence the accessibility of the mineral to microorganisms and the kinetics of metal extraction.

5.2 Methodology

The ferric ion precipitates under examination in this segment were derived from the experiments conducted in Chapter 4. The characterization techniques employed in this research were comprehensively outlined in Sections 3.6.1, 3.6.2, 3.6.3, and 3.6.4 of Chapter 3. Within the framework of this thesis, the precipitate samples were synthesized at the specified solution temperatures of 30, 35, and 40 °C, respectively.

5.3 Results and Discussion

5.3.1 X-ray diffraction (XRD) analysis

The X-ray diffraction pattern alongside the elemental composition of the precipitates, as depicted in Figure 5.1, is presented. The X-ray diffraction analyses, as illustrated in Figure 5.1, demonstrate that the precipitates synthesized within the temperature range under

investigation display uniformity. Moreover, as illustrated in Figure 5.1b, the compounds of precipitates synthesized during the process at the examined temperatures do not display additional peaks indicative of different forms of jarosite (hematite, goethite, etc.). The patterns depicted in Figure 5.1 correspond with the X-ray Diffraction (XRD) reflections of potassium jarosite (K-jarosite), [$KFe_3(SO_4)_2(OH)_6$], wherein the (113) orientation is identified as the most favoured. These crystals crystallize in the rhombohedral system (R3m Spatial Group). Moreover, it's apparent that every diffraction peak displays a comparable pattern, indicating that the temperature change had a minimal impact on the crystal's strain, possibly playing a role in their ability to retain a crystalline structure. Scherrer's equation was used to determine the average crystallite sizes (Equation 3.1) (Holzwarth & Gibson, 2011; Oladipo, 2022) and was measured at 19.85, 17.21, and 19.34 nm for temperatures of 30, 35, and 40 °C respectively as shown in Table 5.1. It was noted that as the temperature of the solution was elevated, there was a corresponding reduction in the average crystallite size. This trend is expected due to the diminished dominance of OH^- ions in comparison to SO_4^{2-} ions within the jarosite structure, as the OH^- ion has a smaller ionic radius (r_{OH^-} = 0.119 nm < $r_{SO_4^{2-}}$ = 0.244 nm), this smaller ionic radius may facilitate the decrease in crystallite size (Oladipo, 2022).

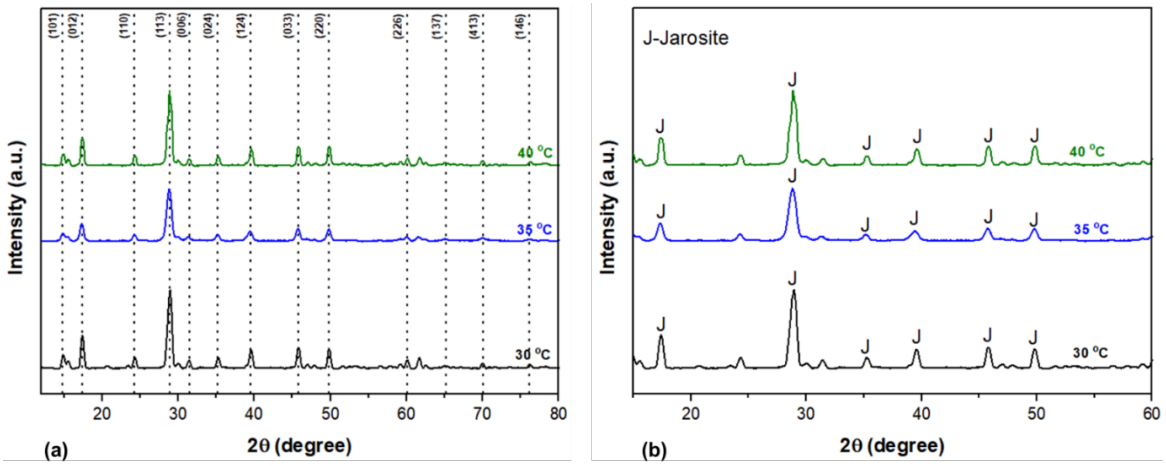

Figure 5.1: XRD patterns of potassium jarosites

Table 5.1: Size of crystal and lattice parameters of the generated jarosite at different temperatures

Jarosite sample	Average crystallite size (nm)	a=b (Å)*	c (Å)
30 °C	19.85	7.31	17.03
35 °C	17.21		
40 °C	19.34		

*a=b trigonal (hexagonal) lattice

5.3.2 SEM analysis

Figure 5.3 displays SEM images of the precipitates that have been formed at different temperatures. The precipitate morphologies in this study exhibited some variation, yet, generally, they resembled potassium-jarosite. All the precipitates that were formed were characterized by their dense, light ochreous yellow residues, as depicted in Figure 4.4. These morphological features are indicative of potassium jarosite, distinguished by clusters of spherical, elliptical, and/or rectangular, granular particles, lacking any notable sharp edges. According to Sasaki et al. (2006) and Oladipo, (2022) the distinct crystalline nature of the tabular and round shapes observed can be attributed to the presence of large cell concentrations.

According to Dutrizac & Chen, (2008), research suggests that rising temperatures can facilitate an increase in the conversion of minerals belonging to the jarosite group. Consequently, this increase in precipitate formation has been associated with a reduction in agglomeration and an increase in particle density. Furthermore, the acidic character of the solution has been identified as another contributing factor to the decrease in agglomeration. This can be explained by the fact that the addition of a strong base (NaOH), primarily potassium (K^+) and hydroxide (OH^-) ions, raises the pH of the solution. These OH^- ions then occupy the surface facets of the formed nuclei, thereby inhibiting the development and agglomeration of particles (Hernández-Lazcano et al., 2021; Oladipo, 2022).

Furthermore, the presence of crust-like, small to tiny particles clustered on the surfaces of individual particles was observed. The particles on precipitates formed across all samples, and were notably more abundant in the precipitate formed at a temperature of 30 ^oC. This phenomenon may be attributed to a reduced precipitation rate and a potentially diminished concentration of cell numbers, which could have been involved in the formation of unripened crystals.

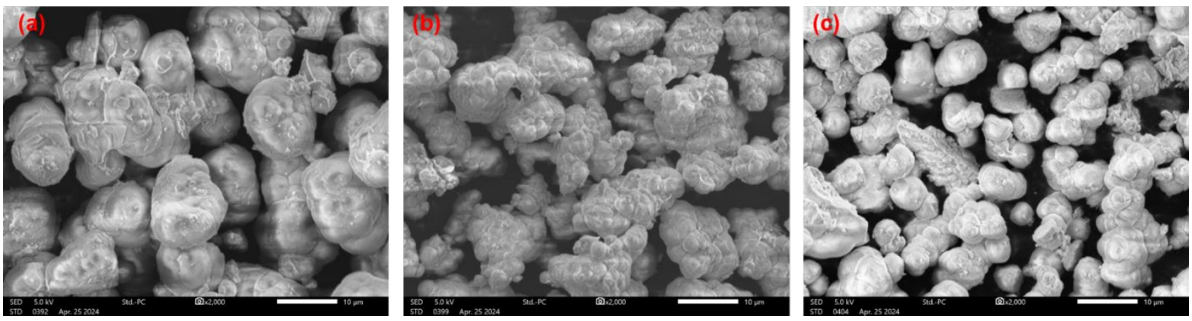

Figure 5.2: SEM images of potassium jarosite a) at 30 ^oC, b) at 35 ^oC, and c) at 40 ^oC

5.3.3 FTIR analysis

Figure 5.3 presents the FTIR spectra collected to identify the functional groups present within the synthesized ferric ion precipitates. It is observed that there is a notable degree of similarity among the spectral peaks. Specifically, the spectral bands falling within the range of 3361 – 3362 cm^{-1} are assigned to the νOH stretching vibrational mode in jarosite. This assignment is attributed to the presence of water and hydroxyl groups, which serve as the origin of the spectral activity in this mode (Sasaki et al., 1998).

Bands observed between 1625 – 1635 cm^{-1} correspond to the δ(H_2O), indicating water-bending vibrations. The spectral bands within the regions 1185 – 1188 cm^{-1} and 1081 – 1083 cm^{-1} are associated with the $\nu 3(SO_4^{2-})$ stretching vibration (Bishop & Murad, 2005). It has been observed that the bands located approximately at 1100 cm^{-1} exhibit sensitivity to cations. The spectral bands observed between 1077 and 1080 cm^{-1} exhibit a close alignment with prior findings concerning K-jarosite (Spratt et al., 2013). The identification of strong bands within the specified region, spanning from 988 to 991 cm^{-1}, is attributed to the stretching vibrational modes of $\nu 1(SO_4^{2-})$ and OH deformation (δOH) (Oladipo, 2022). The distinct bands observed at 625 - 627 cm^{-1} correspond to the bending vibrational mode of $\nu 4(SO_4^{2-})$ within jarosite. The spectral bands at lower energies, ranging from 464 – 502 cm^{-1}, are attributed to the Fe–O lattice stretching vibrational mode of FeO_6 octahedral component within jarosite crystals (Breitinger et al., 1997). It is important to note that the $\nu 2(SO_4^{2-})$, a bending vibrational mode, was not observed, presumably owing to its overlap with adjacent high absorption modes (Zhu et al., 2013).

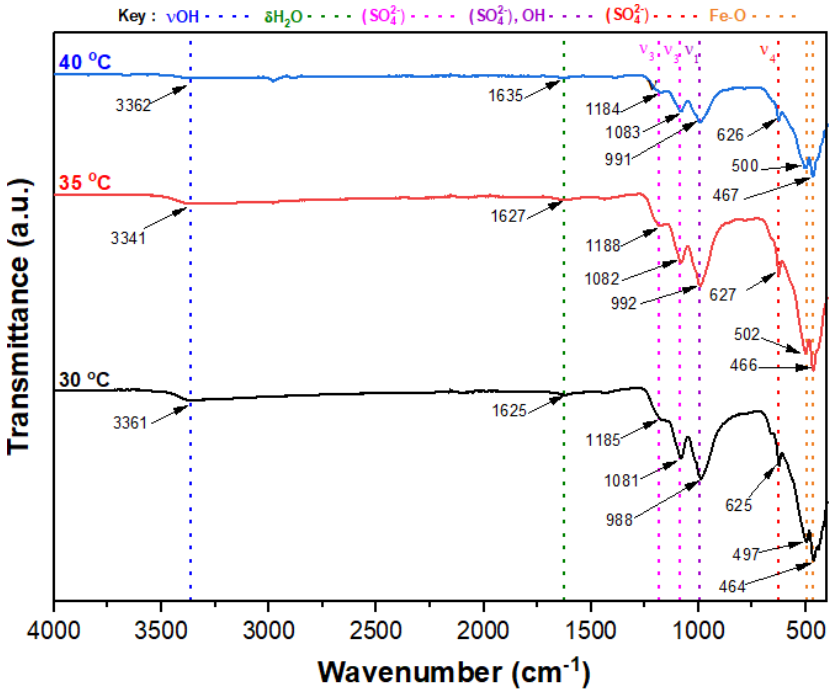

Figure 5.3: FTIR spectra of potassium jarosite

5.3.4 TGA analysis

The detailed profiles of the thermal decomposition of K-Jarosite, as shown in Figure 5.4 (a-c) of the first derivative thermogravimetry analysis (DTA) and TGA profiles display significant similarities. However, it has been noted that there exist nuanced differences in the location and magnitude of specific endothermic peaks.

Across all profiles, the mass loss occurred in three distinct phases, characterized by five notable endothermic peaks. The initial endothermic peak was observed at 0.18% (30 °C), 14.07% (35 °C), and 12.04% (40 °C) of the sample's volume, accompanied by both weak and strong endothermic peaks at temperatures of 30 °C were 170 °C, and 395 °C respectively. Similarly, at 35 °C, the peaks were observed at temperatures of 170 °C and 395 °C. Lastly, at 40 °C, the peaks were noted at temperatures of 244 °C and 406 °C. These peaks correspond to the processes of dehydroxylation and the desorption of water molecules adsorbed onto potassium jarosite, which subsequently leads to the formation of compounds resembling yavapaiite. Additionally, the samples displayed an endothermic peak at a position close to the others, which can be attributed to the crystallization of hematite (α-Fe2O3) (Zhu et al., 2013; Oladipo, 2022). The following equation summarizes this process:

$$KFe_3(SO_4)_2(OH)_6 \rightarrow KFe(SO_4)_2 + Fe_2O_3 + 3H_2O \quad 5.1$$

The highest point and strength of the endothermic maximum are fairly uniform across the samples. This peak is reached at temperatures of 709 °C for (30 °C); 705 °C (35 °C), and finally, at 710 °C (40 °C). This peak is accompanied by a decrease in weight of 0.22%, 18.21%, and 15.07% at temperatures of 30 °C, 35 °C, and 40 °C, respectively. This occurrence is attributed to the thermal decomposition of yavapaiite-type structures (Zhu et al., 2013) and the emission of sulphur oxides (Jiménez et al., 2019), as shown:

$$KFe(SO_4)_2 \rightarrow 1/2Fe_2O_3 + 1/2K_2SO_4 + SO_{3(g)} \quad 5.2$$

Moreover, the highest heat absorption peaks at 829 °C (30 °C), 830 °C (35 °C), and 836 °C (40 °C), which indicate the third significant weight losses of 0.08% (30 °C), 6.8% (35 °C), and 6.33% (40 °C) respectively, suggest the breakdown of certain intermediate substances. Furthermore, these results highlight the predominant amounts of K_2SO_4 and α-Fe_2O_3 (Drouet & Navrotsky, 2003). Moreover, Drouet & Navrotsky (2003), noted that the observed breakdown occurred across a variety of temperatures in Figure 5.4(a–c), possibly due to the influence of reaction rates and the distribution of particle sizes.

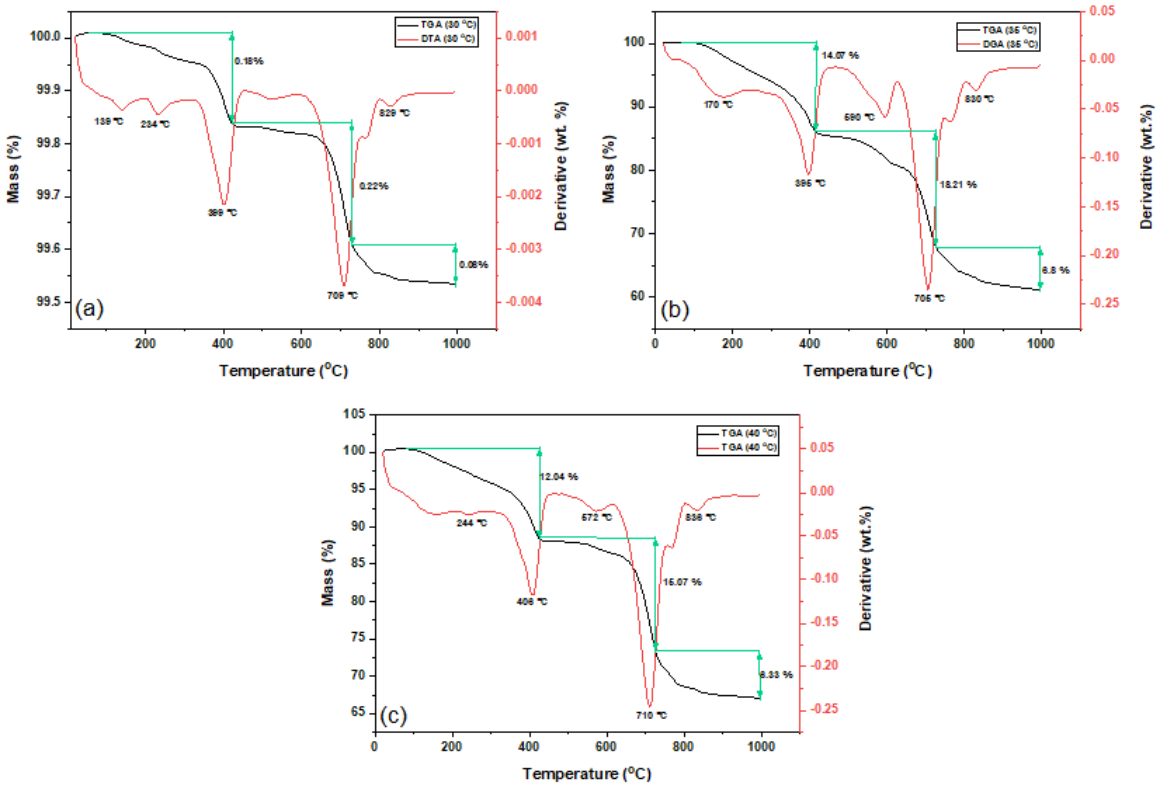

Figure 5.4: Potassium jarosite analysis by TGA/DTA

5.4 Conclusion

This chapter explored the analysis of the influence of temperature on the characteristics of the surface of ferric-ion precipitates generated throughout the biooxidation process involving ferrous ions. The precipitates were thoroughly examined utilising a combination of scanning electron microscopy (SEM), Fourier transform infrared spectroscopy (FTIR), X-ray diffraction (XRD), and Thermogravity analysis (TGA).

The X-ray Diffraction (XRD) patterns of the synthesized crystals were identified as potassium jarosite, potassium ferric sulfate hexahydrate [$KFe_3(SO_4)_2(OH)_6$], and the preferred orientation was (113). Furthermore, no alternative forms of substances with suboptimal or optimal crystalline structures, such as hematite or goethite, were discovered. The SEM studies revealed that the formed crystals looked like potassium jarosite, made up of clusters of spherical, oval, and granular shapes. Spherical particles with a crust-like appearance were seen on the surfaces of these particles, which were more common at 30 °C, likely due to a slower formation process and fewer cell structures. The FTIR spectra of the iron ion crystals showed similar spectral patterns to those reported for potassium jarosite. The thermal decomposition profiles of potassium jarosite showed minor differences in the endothermic peaks. These peaks were related to the removal of water molecules, resulting in the creation of compounds similar to yavapaiite. The peaks with the highest absorption at 829, 830, and

836 °C indicated significant weight losses as the temperature increased. To conclude, reduced crystallite size and increased surface area are exhibited by the jarosite produced at various temperatures. This could facilitate the movement of metal ions across the jarosite and the adsorption of these ions onto its surface during bioleaching, thus obstructing the effective recovery of the desired metal.

Chapter 6: CONCLUSIONS AND RECOMMENDATIONS

6.1 Conclusions

Studies indicate that the formation of precipitates acts as a mechanism for the elimination of undesirable iron, sulfate ions, or alkali ions from the system. Although it is possible to minimize the formation of precipitates, a notable buildup over time can result in slower reactions and diminish the effectiveness of bioleaching processes by ensnaring the target metals within the precipitate residue. Furthermore, the characterization of ferric-ion precipitates, quantification studies, and the impact of low temperatures on precipitate formation have been conducted. Nonetheless, there remains a significant lack of information regarding the kinetics of ferric-ion precipitation. The goal of this research was to explore the kinetics of iron precipitation during microbial ferrous-ion oxidation in shake flasks and to understand how temperature affects the kinetics of ferric-ion precipitates. This was accomplished by the following approaches: (i) The effect of varying operating temperatures on the kinetics of ferric-ion precipitation was investigated. (ii) Changes in ferric-ion concentrations at various temperatures were observed to determine whether there exists a threshold concentration for precipitation to occur. (iv) Estimation of activation energy and thermodynamic parameters of the precipitates obtained during the experiment. (v) Characterization studies were conducted on the generated precipitates to determine their properties.

During the investigation into ferric precipitation, as outlined in Chapter 4, it was found that ferric precipitates increased with increasing temperatures and an increase in rate constant. The study demonstrated that ferric-ion precipitates formed within the temperature range examined. Additionally, their presence became apparent after 24 hours of operation at an average threshold concentration of 1.22 g/L and was characterised by the formation of yellow solids. It is necessary to acknowledge that the quantity of precipitates formed at this stage was relatively small compared to the amount generated at the experiment's conclusion, which was also higher than in some other studies. The findings from thermodynamics indicated that the process of precipitate formation was non-spontaneous and would require a substantial amount of energy to achieve spontaneity.

In Chapter 5, the influence of temperature on the surface characteristics of iron precipitates generated through microbial oxidation was examined. The patterns obtained through X-ray diffraction analysis indicate that the precipitates observed in this study were predominantly composed of potassium jarosite. The research demonstrated a consistent decrease in crystallite size, ranging from 19.85 to 17.21 nm, as the temperature increased. Furthermore, SEM analyses revealed that the precipitates exhibited clusters of spherical, oval, and granular shapes, with a crust-like appearance on their surfaces. The FTIR spectra confirmed the

presence of functional groups characteristic of K-jarosite crystals. Regarding thermal stability, TGA studies indicated that K-jarosite underwent dehydroxylation between 395 and 406 °C, while yavapaiite experienced complete thermal decomposition between 705 and 710 °C. It was determined that changes in operating temperature led to a reduction in crystallite size and an enhancement in surface area. This, in turn, facilitated the movement of metal ions and the adsorption process during bioleaching, thereby impeding the efficiency of metal extraction.

6.2 Recommendations

This study aimed to explore the kinetics of precipitates that are produced during the microbial oxidation of ferrous ions. The investigations were conducted in shake flasks which to a certain extent does not. It is necessary to acknowledge that, in addition to temperature changes, the microbial consortia employed, the precipitation of ferric ions, and various operating parameters in a heap leaching process, such as packing height and size, solution pH, and the presence of different metals in the ore particles, also play significant roles in the limitations of microbial kinetics. As a result, the following recommendations for future research are proposed.

- This study focused on a temperature range that fosters mesophilic growth. However, the temperature within the industrial heap can vary significantly, ranging from as low as 10°C on the surface in areas where the ambient temperature is low, to temperatures exceeding 65°C deeper within the heap, which encourages the growth of extreme thermophiles. As a result, it is recommended that further research be conducted on a broader temperature range and the simulation of heap settings. This will help to enhance our understanding of microbial ferrous-ion oxidation, which mimics real-world heap conditions.

- The formation of precipitates during biooxidation processes is heavily influenced by both kinetic and thermodynamic factors. In this study, the kinetic and thermodynamic factors of ferric-ion precipitates were experimentally measured. Nonetheless, further works on the thermodynamic and kinetic data for precipitates and jarosite minerals will need to be investigated further in upcoming studies to provide more clarity on its implication in a typical biohydrometallurgical process. Additionally, the reliable determination of the formation enthalpies and entropies of jarosite samples will also be required.

- The study used microorganisms of mesophilic consortia, which are acidophilic and possess the ability to metabolize iron and convert inorganic sulphur compounds into

soluble minerals. However, in recent years, there have been notable observations of indigenous microorganisms emerging within microbial communities during both industrial bioleaching processes and laboratory-scale bioleaching. This has led to the discovery of novel, specially adapted microorganisms, such as *Cuniculiplasma divulgatum sp.* nov. Consequently, it is recommended that the dynamics and influence of these microorganisms on the formation of precipitates (e.g., jarosites), as well as their impact on the kinetics and thermodynamics of bioleaching and biooxidation processes, should be further explored.

Chapter 7: References

Abdollahi, H., Noaparast, M., Shafaei, S.Z., Akcil, A., Panda, S., Kashi, M.H. & Karimi, P. 2019. Prediction and optimization studies for bioleaching of molybdenite concentrate using artificial neural networks and genetic algorithm. *Minerals Engineering*, 130(September 2018): 24–35. https://doi.org/10.1016/j.mineng.2018.10.008.

Acevedo, F. 2000. The use of reactors in biomining processes. *Electronic Journal of Biotechnology*, 3(3): 184–194.

Ahonen, L. & Tuovinen, O.H. 1989. Microbiological Oxidation of Ferrous Iron at Low Temperatures. *Applied and Environmental Microbiology*, 55(2): 312–316.

Anjum, F., Shahid, M. & Akcil, A. 2012. Biohydrometallurgy techniques of low grade ores: A review on black shale. *Hydrometallurgy*, 117–118: 1–12. http://dx.doi.org/10.1016/j.hydromet.2012.01.007.

Baniasadi, M., Vakilchap, F., Bahaloo-Horeh, N., Mousavi, S.M. & Farnaud, S. 2019. Advances in bioleaching as a sustainable method for metal recovery from e-waste: A review. *Journal of Industrial and Engineering Chemistry*, 76: 75–90. https://doi.org/10.1016/j.jiec.2019.03.047.

Beverskog, B. & Puigdomenech, I. 1996. Revised Diagrams for Iron At 25-300 ° C. *Science*, 38(12): 2121–2135. http://www.sciencedirect.com/science/article/pii/S0010938X96000674.

Bishop, J.L. & Murad, E. 2005. The visible and infrared spectral properties of jarosite and alunite. *American Mineralogist*, 90(7): 1100–1107.

Boon, M., Meeder, T.A., Thöne, C., Ras, C. & Heijnen, J.J. 1999. The ferrous iron oxidation kinetics of Thiobacillus ferrooxidans in batch cultures. *Applied Microbiology and Biotechnology*, 51(6): 820–826.

Bosecker, K. 1997. Bioleaching: Metal solubilization by microorganisms. *FEMS Microbiology Reviews*, 20(3–4): 591–604.

Breitinger, D.K., Krieglstein, R., Bogner, A., Schwab, R.G., Pimpl, T.H., Mohr, J. & Schukow, H. 1997. Vibrational spectra of synthetic minerals of the alunite and crandallite type. *Journal of Molecular Structure*, 408–409: 287–290.

Brierley, C.L. 2008. How will biomining be applied in future? *Transactions of Nonferrous Metals Society of China (English Edition)*, 18(6): 1302–1310. http://dx.doi.org/10.1016/S1003-6326(09)60002-9.

Brierley, C.L. & Brierley, J.A. 2013. Progress in bioleaching: Part B: Applications of microbial processes by the minerals industries. *Applied Microbiology and Biotechnology*, 97(17): 7543–7552.

Brierley, J.A. & Brierley, C.L. 2001. Present and future commercial applications of biohydrometallurgy. : 233–239.

Brock, T.D. & Gustafson, J. 1976. Ferric iron reduction by sulfur- and iron-oxidizing bacteria. *Applied and environmental microbiology*, 32(4): 567–571.

Chowdhury, F. 2012. *The effect of temperature on the kinetics of microbial ferrous-iron oxidation in a packed column bioreactor by*. Cape Peninsula University of Technology.

Chowdhury, F. & Ojumu, T. V. 2014. Investigation of ferrous-iron biooxidation kinetics by Leptospirillum ferriphilum in a novel packed-column bioreactor: Effects of temperature and jarosite accumulation. *Hydrometallurgy*, 141: 36–42. http://dx.doi.org/10.1016/j.hydromet.2013.09.011.

Chukwuchendo, C.E. 2016. *Bio-oxidation of ferrous iron at low temperature conditions in a packed bed column bioreactors*. Cape Peninsula University of Technology.

Chukwuchendo, E.C. & Ojumu, T.V. 2017. Microbial ferrous ion oxidation versus ferric ion precipitation at low temperature conditions. *Solid State Phenomena*, 262 SSP: 381–384.

Coram, N.J. & Rawlings, D.E. 2002. Molecular relationship between two groups of the genus Leptospirillum and the finding that Leptospirillum ferriphilum sp. nov. Dominates south African commercial biooxidation tanks that operate at 40°C. *Applied and Environmental Microbiology*, 68(2): 838–845.

Córdoba, E.M., Muñoz, J.A., Blázquez, M.L., González, F. & Ballester, A. 2008a. Leaching of chalcopyrite with ferric ion. Part I: General aspects. *Hydrometallurgy*, 93(3–4): 81–87.

Córdoba, E.M., Muñoz, J.A., Blázquez, M.L., González, F. & Ballester, A. 2008b. Leaching of chalcopyrite with ferric ion. Part II: Effect of redox potential. *Hydrometallurgy*, 93(3–4): 88–96.

Crundwell, F.K. 2003. How do bacteria interact with minerals? *Hydrometallurgy*, 71(1–2): 75–81.

Daoud, J. & Karamanev, D. 2006. Formation of jarosite during Fe2+ oxidation by Acidithiobacillus ferrooxidans. *Minerals Engineering*, 19(9): 960–967.

Das, T., Ayyappan, S. & Roy Chaudhury, G. 1999. Factors affecting bioleaching kinetics of sulfide ores using acidophilic micro-organisms. *BioMetals*, 12(1): 1–10.

Dopson, M., Baker-Austin, C., Koppineedi, P.R. & Bond, P.L. 2003. Growth in sulfidic mineral environments: Metal resistance mechanisms in acidophilic micro-organisms. *Microbiology*, 149(8): 1959–1970.

Dopson, M., Halinen, A.-K., Rahunen, N., Zkaya, B.O., Sahinkaya, E., Kaksonen, A.H., Lindstro¨m, E.B. & JPuhakka, aakko A. 2007. Mineral and Iron Oxidation at Low Temperatures by Pure and Mixed Cultures of Acidophilic Microorganisms. *Journal of anatomy*, 97: 503–505.

Drouet, C. & Navrotsky, A. 2003. Synthesis, characterization, and thermochemistry of K-Na-H3O jarosites. *Geochimica et Cosmochimica Acta*, 67(11): 2063–2076.

Dutrizac, J.E. & Chen, T.T. 2008. Behaviour of the alkaline earth elements (beryllium to radium) during the precipitation of jarosite-type compounds. *Canadian Metallurgical Quarterly*, 47(4): 387–402.

Eftekhari, N., Kargar, M., Zamin, F.R., Rastakhiz, N. & Manafi, Z. 2020. A review on various aspects of jarosite and its utilization potentials. *Annales de Chimie: Science des Materiaux*, 44(1): 43–52.

Encinar, J.M., Pardal, A. & Sánchez, N. 2016. An improvement to the transesterification process by the use of co-solvents to produce biodiesel. *Fuel*, 166(November): 51–58.

Franzmann, P.D., Haddad, C.M., Hawkes, R.B., Robertson, W.J. & Plumb, J.J. 2005. Effects of temperature on the rates of iron and sulfur oxidation by selected bioleaching Bacteria and Archaea: Application of the Ratkowsky equation. *Minerals Engineering*, 18(13–14): 1304–1314.

Gahan, C.S., Srichandan, H., Kim, D.-J. & Akcil, A. 2012. Biohydrometallurgy and biomineral processing technology: a review on its past, present and future. *Research Journal of Recent Sciences*, 1(10): 85–99.

Gentina, J.C. & Acevedo, F. 2016. Copper bioleaching in Chile. *Minerals*, 6(1).

Gramp, J.P., Jones, F.S., Bigham, J.M. & Tuovinen, O.H. 2008. Monovalent cation concentrations determine the types of Fe(III) hydroxysulfate precipitates formed in bioleach solutions. *Hydrometallurgy*, 94(1–4): 29–33.

Grishin, S.I., Bigham, J.M. & Tuovinen, O.H. 1988. Characterization of Jarosite Formed upon Bacterial Oxidation of Ferrous Sulfate in a Packed-Bed Reactor. *Applied and Environmental Microbiology*, 54(12): 3101–3106.

Hansford, G.S. & Vargas, T. 2001. Chemical and electrochemical basis of bioleaching

processes. *Hydrometallurgy*, 59: 135–145.

Harvey, P.I. & Crundwell, F.K. 1997. Growth of Thiobacillus ferrooxidans: A novel experimental design for batch growth and bacterial leaching studies. *Applied and Environmental Microbiology*, 63(7): 2586–2592.

Hernández-Lazcano, E., Cerecedo-Sáenz, E., Hernández-ávila, J., Toro, N., Karthik, T.V.K., Mendoza-Anaya, D., Fernández-García, M.E., Rodríguez-Lugo, V. & Salinas-Rodríguez, E. 2021. Synthesis of hydronium-potassium jarosites: The effect of ph and aging time on their structural, morphological, and electrical properties. *Minerals*, 11(1): 1–15.

van Hille, R.P., van Zyl, A.W., Spurr, N.R.L. & Harrison, S.T.L. 2010. Investigating heap bioleaching: Effect of feed iron concentration on bioleaching performance. *Minerals Engineering*, 23(6): 518–525. http://dx.doi.org/10.1016/j.mineng.2010.01.011.

Hofer, E. & Steininger, R. 2023. Does it occur or not ? – A structured approach to support students in determining the spontaneity of chemical reactions. *Chemistry Teacher International*: 1–17. https://doi.org/10.1515/cti-2022-0046.

Holzwarth, U. & Gibson, N. 2011. The Scherrer equation versus the 'Debye-Scherrer equation' *Nature Publishing Group*, 6(9): 534. http://www.nature.com/doifinder/10.1038/nnano.2011.145%5Cnpapers2://publication/doi/10.1038/nnano.2011.145.

Jafari, M., Abdollahi, H., Shafaei, S.Z., Gharabaghi, M., Jafari, H., Akcil, A. & Panda, S. 2019. Acidophilic bioleaching: A Review on the Process and Effect of Organic–inorganic Reagents and Materials on its Efficiency. *Mineral Processing and Extractive Metallurgy Review*, 40(2): 87–107.

Jiménez, A., Hernández, A. & Prieto, M. 2019. Crystallization behaviour of iron-hydroxide sulphates by aging under ambient temperature conditions. *Minerals*, 9(1).

Jin, J., Shi, S.Y., Liu, G.L., Zhang, Q.H. & Cong, W. 2013. Comparison of Fe2+ oxidation by Acidithiobacillus ferrooxidans in rotating-drum and stirred-tank reactors. *Transactions of Nonferrous Metals Society of China (English Edition)*, 23(3): 804–811. http://dx.doi.org/10.1016/S1003-6326(13)62532-7.

Kahrizi, E., Alemzadeh, I. & Vossoughi, M. 2009. Bio-oxidation of ferrous ions by Acidithioobacillus ferrooxidans in amonolithic bioreactor. *Journal of Chemical Technology and Biotechnology*, 84(4): 504–510.

Kaksonen, A.H., Morris, C., Rea, S., Li, J., Usher, K.M., McDonald, R.G., Hilario, F., Hosken,

T., Jackson, M. & Du Plessis, C.A. 2014. Biohydrometallurgical iron oxidation and precipitation: Part II - Jarosite precipitate characterisation and acid recovery by conversion to hematite. *Hydrometallurgy*, 147–148: 264–272. http://dx.doi.org/10.1016/j.hydromet.2014.04.015.

Kaksonen, A.H., Morris, C., Rea, S., Li, J., Wylie, J., Usher, K.M., Ginige, M.P., Cheng, K.Y., Hilario, F. & Du Plessis, C.A. 2014. Biohydrometallurgical iron oxidation and precipitation: Part i - Effect of pH on process performance. *Hydrometallurgy*, 147–148: 255–263. http://dx.doi.org/10.1016/j.hydromet.2014.04.016.

Kazadi, T.K. 2007. *Evaluation of the Redostat Device for the Study of Ferrous Iron Biological Oxidation Kinetics*. University of Cape Town.

Kupka, D., Rzhepishevska, O.I., Dopson, M., Lindstro¨m, E.B. rje, Karnachuk, O. V. & Tuovinen, O.H. 2007. Bacterial Oxidation of Ferrous Iron at Low Temperatures. *Biotechnology and bioengineering*, 97: 1470–1478.

Leahy, M.J., Davidson, M.R. & Schwarz, M.P. 2005. A two-dimensional CFD model for heap bioleaching of chalcocite. *ANZIAM Journal*, 46: 439.

Liao, Y., Zhou, L., Bai, S., Liang, J. & Wang, S. 2009. Occurrence of biogenic schwertmannite in sludge bioleaching environments and its adverse effect on solubilization of sludge-borne metals. *Applied Geochemistry*, 24(9): 1739–1746. http://dx.doi.org/10.1016/j.apgeochem.2009.05.003.

Liu, J., Li, B., Zhong, D., Xia, L. & Qiu, G. 2007. Preparation of jarosite by Acidithiobacillus ferrooxidans oxidation LIU. : 623–628.

Liu, J. yan, Xiu, X. xiang & Cai, P. 2009. Study of formation of jarosite mediated by thiobacillus ferrooxidans in 9K medium. *Procedia Earth and Planetary Science*, 1(1): 706–712. http://dx.doi.org/10.1016/j.proeps.2009.09.111.

Mabusela, B. & Ojumu, T.V. 2017. The effect of initial solution ph on surface properties of ferric ion precipitates formed during biooxidation of ferrous ion by Leptospirillum ferriphilum. *Solid State Phenomena*, 262 SSP: 403–407.

Mabusela, B.P. 2017. *The effect of initial pH on surface properties of ferric ion precipitates formed during microbial oxidation of ferrous ion by Leptospirillum ferriphilum in a CSTR*. Cape Peninsula University of Technology.

Mazuelos, A., Palencia, I., Romero, R., Rodríguez, G. & Carranza, F. 2001. Ferric iron production in packed bed bioreactors: Influence of pH, temperature, particle size,

bacterial support material and type of air distributor. *Minerals Engineering*, 14(5): 507–514.

Morin, D.H.R. & D'Hugues, P. 2007. Bioleaching of a cobalt-containing pyrite in stirred reactors: A case study from laboratory scale to industrial application. *Biomining*: 35–55.

Mulligan, C.N., Kamali, M. & Gibbs, B.F. 2004. Bioleaching of heavy metals from a low-grade mining ore using Aspergillus niger. *Journal of Hazardous Materials*, 110(1–3): 77–84.

Nazari, B., Jorjani, E., Hani, H., Manafi, Z. & Riahi, A. 2014. Formation of jarosite and its effect on important ions for Acidithiobacillus ferrooxidans bacteria. *Transactions of Nonferrous Metals Society of China (English Edition)*, 24(4): 1152–1160. http://dx.doi.org/10.1016/S1003-6326(14)63174-5.

Nemati, M., Harrison, S.T.L., Hansford, G.S. & Webb, C. 1998. Biological oxidation of ferrous sulphate by Thiobacillus ferrooxidans: A review on the kinetic aspects. *Biochemical Engineering Journal*, 1(3): 171–190.

Nurmi, P., Özkaya, B., Sasaki, K., Kaksonen, A.H., Riekkola-Vanhanen, M., Tuovinen, O.H. & Puhakka, J.A. 2010. Biooxidation and precipitation for iron and sulfate removal from heap bioleaching effluent streams. *Hydrometallurgy*, 101(1–2): 7–14. http://dx.doi.org/10.1016/j.hydromet.2009.11.004.

Ojumu, T. 2008. *The Effects of Solution Conditions on the Kinetics of Microbial Ferrous-Iron Oxidation by Leptospirillum Ferriphilum in Continuous Culture*. University of Cape Town.

Ojumu, T. V., Hansford, G.S. & Petersen, J. 2009. The kinetics of ferrous-iron oxidation by Leptospirillum ferriphilum in continuous culture: The effect of temperature. *Biochemical Engineering Journal*, 46(2): 161–168.

Ojumu, T. V. & Petersen, J. 2011. The kinetics of ferrous ion oxidation by Leptospirillum ferriphilum in continuous culture: The effect of pH. *Hydrometallurgy*, 106(1–2): 5–11. http://dx.doi.org/10.1016/j.hydromet.2010.11.007.

Ojumu, T. V., Petersen, J., Searby, G.E. & Hansford, G.S. 2006. A review of rate equations proposed for Ojumu, T. V., Petersen, J., Searby, G. E., & Hansford, G. S. (2006). A review of rate equations proposed for microbial ferrous-iron oxidation with a view to application to heap bioleaching. Hydrometallurgy, 83(1–4),. *Hydrometallurgy*, 83(1–4): 21–28.

Oladipo, B. 2022. *FERRIC PRECIPITATION AND METAL SORPTION IN BIOHYDROMETALLURGICAL PROCESSES*. Cape Peninsula University of Technology.

Oladipo, B., Govender-Opitz, E. & Ojumu, T. V. 2021. Kinetics , Thermodynamics , and Mechanism of Cu (II) Ion Sorption by Biogenic Iron Precipitate : Using the Lens of Wastewater Treatment to Diagnose a Typical Biohydrometallurgical Problem. , (Ii): 10.

Olson, G.J., Brierley, J.A. & Brierley, C.L. 2003. Bioleaching review part B: Progress in bioleaching: Applications of microbial processes by the minerals industries. *Applied Microbiology and Biotechnology*, 63(3): 249–257.

Ozkaya, B., Sahinkaya, E., Nurmi, P., Kaksonen, A.H. & Puhakka, J.A. 2007. Iron oxidation and precipitation in a simulated heap leaching solution in a Leptospirillum ferriphilum dominated biofilm reactor. *Hydrometallurgy*, 88(1–4): 67–74.

Panda, S., Akcil, A., Pradhan, N. & Deveci, H. 2015. Current scenario of chalcopyrite bioleaching: A review on the recent advances to its heap-leach technology. *Bioresource Technology*, 196: 694–706.

Panda, S., Biswal, A., Mishra, S., Panda, P.K., Pradhan, N., Mohapatra, U., Sukla, L.B., Mishra, B.K. & Akcil, A. 2015. Reductive dissolution by waste newspaper for enhanced meso-acidophilic bioleaching of copper from low grade chalcopyrite: A new concept of biohydrometallurgy. *Hydrometallurgy*, 153: 98–105. http://dx.doi.org/10.1016/j.hydromet.2015.02.006.

Panda, S., Sanjay, K., Sukla, L.B., Pradhan, N., Subbaiah, T., Mishra, B.K., Prasad, M.S.R. & Ray, S.K. 2012. Insights into heap bioleaching of low grade chalcopyrite ores - A pilot scale study. *Hydrometallurgy*, 125–126: 157–165. http://dx.doi.org/10.1016/j.hydromet.2012.06.006.

Petersen, J. & Ojumu, T.V. 2007. The Effect of Total Iron Concentration and Iron Speciation on the Rate of Ferrous Iron Oxidation Kinetics of *Leptospirillum ferriphilum* in Continuous Tank Systems. *Advanced Materials Research*, 20–21: 447–451.

Plumb, J.J., Gibbs, B., Stott, M.B., Robertson, W.J., Gibson, J.A.E., Nichols, P.D., Watling, H.R. & Franzmann, P.D. 2002. Enrichment and characterisation of thermophilic acidophiles for the bioleaching of mineral sulphides. *Minerals Engineering*, 15(11): 787–794.

Plumb, J.J., Muddle, R. & Franzmann, P.D. 2008. Effect of pH on rates of iron and sulfur oxidation by bioleaching organisms. *Minerals Engineering*, 21(1): 76–82.

Pradhan, N., Nathsarma, K.C., Srinivasa Rao, K., Sukla, L.B. & Mishra, B.K. 2008. Heap bioleaching of chalcopyrite: A review. *Minerals Engineering*, 21(5): 355–365.

Qiu, M.Q., Xiong, S.Y., Zhang, W.M. & Wang, G.X. 2005. A comparison of bioleaching of chalcopyrite using pure culture or a mixed culture. *Minerals Engineering*, 18(9): 987–990.

Rawlings, D.E. 2005. Characteristics and adaptability of iron- and sulfur-oxidizing microorganisms used for the recovery of metals from minerals and their concentrates. *Microbial Cell Factories*, 4: 1–15.

Rawlings, D.E. 2002. Heavy metal mining using microbes. *Annual Review of Microbiology*, 56(February 2002): 65–91.

Roger, B. & Herbert, J. 1997. Properties of goethite and jarosite precipitated from acidic groundwater, Dalarna, Sweden. *Clays and Clay Minerals*, 45(2): 261–273.

Roy, S. & Roy, M. 2015. Bioleaching of Heavy Metals by Sulfur Oxidizing Bacteria: A Review. *International Research Journal of Environment Sciences*, 4(9): 1–5.

Sasaki, K., Tanaike, O. & Konno, H. 1998. Distinction of jarosite-group compounds by Raman spectroscopy. *Canadian Mineralogist*, 36(5): 1225–1235.

Seitkamal, K.N., Zhappar, N., Shaikhutdinov, V., Shibayeva, A. & Sagyndykov, U. 2020. A comparative study on psychrophilic and mesophilic biooxidation of ferrous iron by pure cultures of Acidithiobacillus ferrooxidans and Acidithiobacillus ferrivorans. *Bulletin of the Karaganda University. "Biology, medicine, geography Series"*, 99(3): 128–133.

Shuler, M.L. & Kargi, F. 2002. *Bioprocess engineering: Basic concepts*. Second Edi. Prentice-Hall, Inc.

Sowers, T.D., Blackmon, M.D., Betts, A.R., Jerden, M.L., Scheckel, K.G. & Bradham, K.D. 2023. Potassium jarosite seeding of soils decreases lead and arsenic bioaccessibility: A path toward concomitant remediation. *Proceedings of the National Academy of Sciences*, 120: 8. https://doi.org/10.1073/pnas.2311564120.

Spratt, H.J., Rintoul, L., Avdeev, M. & Martens, W.N. 2013. The crystal structure and vibrational spectroscopy of jarosite and alunite minerals. *American Mineralogist*, 98(10): 1633–1643.

Szubert, A., Lupinski, M. & Sadowski, Z. 2006. Application of Shrinking Core Model To Bioleaching of Black Shale Particles. *Physicochemical problems of mineral processing*, 40: 211–225.

Tekin, D. & Yoruk, S. 2013. The effect of ph on rate of bacterial oxidation of Fe (II) by Acidithiobacillus ferrooxidans. *Journal of Selcuk University Natural and Applied …*, 46(1): 117–119. http://www.josunas.org/login/index.php/josunas/article/view/210.

Third, K.A., Cord-Ruwisch, R. & Watling, H.R. 2000. Role of iron-oxidizing bacteria in stimulation or inhibition of chalcopyrite bioleaching. *Hydrometallurgy*, 57(3): 225–233.

Vishniac, W. & Santer, M. 1957. The thiobacilli. *Bacteriological Reviews*, (21): 195–213.

Wang, H., Bigham, J.M. & Tuovinen, O.H. 2006. Formation of schwertmannite and its transformation to jarosite in the presence of acidophilic iron-oxidizing microorganisms. *Materials Science and Engineering C*, 26(4): 588–592.

Wanjiya, M. 2013. *Investigation of bacterial ferrous iron oxidation kinetics in a novel packed-column reactor : pH and jarosite management*. Cape Peninsula University of Technology.

Wanjiya, M., Chowdhury, F. & Ojumu, T.V. 2015. Solution pH and Jarosite Management during Ferrous Iron Biooxidation in a Novel Packed-Column Bioreactor. *Advanced Materials Research*, 1130: 291–295.

Watling, H.R. 2006. The bioleaching of sulphide minerals with emphasis on copper sulphides - A review. *Hydrometallurgy*, 84(1–2): 81–108.

Wu, Z.L., Zou, L.C., Chen, J.H., Lai, X.K. & Zhu, Y.G. 2016. Column bioleaching characteristic of copper and iron from Zijinshan sulfide ores by acid mine drainage. *International Journal of Mineral Processing*, 149: 18–24. http://dx.doi.org/10.1016/j.minpro.2016.01.015.

Yujian, W., Xiaojuan, Y., Wei, T. & Hongyu, L. 2007. High-rate ferrous iron oxidation by immobilized Acidithiobacillus ferrooxidans with complex of PVA and sodium alginate. *Journal of Microbiological Methods*, 68(2): 212–217.

Zhou, D., Wang, L., Chen, X., Wei, X., Liang, J., Zhang, D. & Ding, G. 2018. A novel acid catalyst based on super/subcritical CO2-enriched water for the efficient esterification of rosin. *Royal Society Open Science*, 5(7).

Zhu, J., Gan, M., Zhang, D., Hu, Y. & Chai, L. 2013. The nature of Schwertmannite and Jarosite mediated by two strains of Acidithiobacillus ferrooxidans with different ferrous oxidation ability. *Materials Science and Engineering C*, 33(5): 2679–2685. http://dx.doi.org/10.1016/j.msec.2013.02.026.

Chapter 8: Appendix A: Reagents preparation and determination of concentration of iron species

8.1 Reagents preparation

8.1.1 Spekker acid

The spekker acid solution was prepared by mixing equal volumes of concentrated sulphuric acid (98% H2SO4) and phosphoric acid (85%) with water in a ratio of 3:4 (acid solution: distilled water).

- Measure 600 mL distilled water using a 2 L beaker.
- Carefully add 225 mL of concentrated sulphuric acid (98%) and 225 mL of phosphoric acid (85%) by slowly pouring the acid mixture against the wall of the beaker (Caution: rapid addition of the acid mixture to the distilled water will result in heat of mixing which will cause localised boiling, especially when using concentrated H_2SO_4).
- Allow the mixture to cool to room temperature before transferring into a storage bottle.

8.1.2 Ferric acid

The ferric acid solution was prepared from the spekker acid:

- Measure 600 mL distilled water using a 2 L beaker.
- Slowly and carefully add 150 mL of spekker acid and then 300 mL of concentrated hydrochloric acid (32% HCl) to the distilled water.
- Agitate the mixture using a magnetic stirrer and allow to cool to room temperature before transferring into a storage bottle.

8.1.3 Stannous chloride solution ($SnCl_2$)

- Weigh out 30 g stannous chloride in a 200 mL beaker.
- Add 100 mL concentrated hydrochloric acid (32%) and agitate at 50°C until it dissolves completely.
- Allow to cool to room temperature and dilute with 200 mL distilled water.
- Add a small amount of granular tin to the solution to retard precipitation.

8.1.4 Mercuric Chloride solution ($HgCl_2$)

- Weigh out 50 g mercuric chloride in a 2 L beaker.
- Add 1 L of distilled water and agitate until the solute has dissolved completely (about 2 hours).

- Add a spatula tip of HgCl2 and stir for 2 hours before storage.

8.1.5 Potassium-hydronium Dichromate solution (0.0149 M $K_2Cr_2O_7$)

- Dry approximately 10 g of K2Cr2O7 (Molar mass 294.20 g.mol-1) in an oven at 105 – 110°C for 1 – 2 hours. Cool in a desiccator.
- Accurately weigh out 8.78 g of the dried K2Cr2O7 into a 100 mL beaker.
- Transfer quantitatively into a 2 L beaker.
- Add 1.5 L of distilled water and agitate until dissolved completely.
- Transfer quantitatively into a 2 L standard volumetric flask and fill to the 2 L mark with distilled water.

8.1.6 Barium Diphenylamine Sulphonate (BDS) solution ($C_{24}H_{20}BaN_2O_6S_2$)

- Weigh out 1.0 g of barium diphenylamine sulphonate in a 250 mL beaker and add 100 mL of concentrated sulphuric acid (98%). Agitate until the solute has dissolved completely.

8.2 Determination of ferrous-ion concentration by titration with potassium dichromate solution

- Pipette 5 mL of the required aliquot solution into a 125 mL conical flask.
- Add 10 mL of spekker acid solution.
- Add 2 – 3 drops of BDS indicator.
- Titrate the potassium dichromate (0.0149 M $K_2Cr_2O_7$) solution until the first permanent colour change from yellow to intense purple is obtained.

Ferrous-ion concentration may be calculated using Equation A8.1:

$$Fe^{2+} = \frac{[K_2Cr_2O_7] \times V_T \times (55.84 \times 6)}{V_{solution}} \quad \text{A8.1}$$

Where:

$[Fe^{2+}]$ = Ferrous-ion concentration ($g.L^{-1}$)

$[K_2Cr_2O_7]$ = $K_2Cr_2O_7$ concentration (i.e. 0.0149 M $K_2Cr_2O_7$)

VT = Titration volume (mL) (amount of 0.0149 M $K_2Cr_2O_7$ added)

VSolution = Solution aliquot volume (mL)

8.3 Determination of total iron concentration by titration with potassium dichromate solution

- Filter 5 mL aliquot of sample solution.
- Pipette the required amount of aliquot (i.e. 5 mL) into a 125 mL conical flask.
- Add 10 mL of spekker acid solution and heat until the mixture boils.
- Add stannous (SnCl2) solution dropwise until the yellow colour disappears completely. Add one extra drop and record the amount of stannous chloride added (note: It is important to record this amount, especially when doing duplicate titrations since it gives some an idea of the amount of SnCl2 required for the next duplicate titrations).
- Allow the solution to cool to room temperature and add 10 mL of mercuric chloride (HgCl2) solution. A silky-white precipitate should appear. If no precipitate forms, too little stannous chloride was added in step 4. If the precipitate is heavy and grey/black, too much stannous chloride was added. In either case, abort the experiment and start over.
- Add 3 – 4 drops of barium diphenylamine indicator solution (BDS) and titrate with the potassium dichromate solution until the first permanent colour change from yellow to intense purple is obtained.

Total iron concentration may be calculated using Equation A8.2:

$$Fe^T = \frac{[K_2Cr_2O_7] \times V_T \times (55.84 \times 6)}{V_{solution}} \quad \text{A8.2}$$

Where:

$[Fe^T]$ = Total iron concentration ($g.L^{-1}$)

$[K_2Cr_2O_7]$ = $K_2Cr_2O_7$ concentration (i.e. 0.0149 M $K_2Cr_2O_7$)

VT = Titration volume (mL) (amount of 0.0149 M $K_2Cr_2O_7$ added)

VSolution = Solution aliquot volume (mL)

8.4 Vishniac Trace Metal Solution

Vishniac Trace Metal Solution was prepared according to the method suggested by Vishniac and Santer (1957).

- Weigh the reagents accurately and dilute to 1 L volume with distilled water (dH_2O).
- Prepare 6% potassium hydroxide (KOH) by weighing 15 g KOH and diluting it to 250 mL with dH_2O.

- Dissolve 50 g EDTA (Ethylenediaminetetraacetic acid disodium salt dihydrate) in 200 mL of 6% KOH using a magnetic stirrer.
- In a separate 500 mL beaker weigh the salts listed below and dissolve in 400 mL dH_2O for 30 minutes using a magnetic stirrer.

Table 8. 1: Vishniac Trace Metal Solution chemical list

Chemical	Amount (g)
$CaCl_2.2H_2O$	9.24
$ZnSO_4.7H_2O$	22
$MnCl_2.4H_2O$	5.06
$FeSO_4.7H_2O$	5.0
$(NH_4)_6Mo_7O_{24}.4H_2O$	1.1
$CuSO_4.5H_2O$	1.58
$CoCl_2.6H_2O$	1.62

- Transfer the solution prepared in step 2 quantitatively into the solution prepared in step 3 and make-up to 1 L with dH_2O by rinsing the 500 mL beaker with 400 mL dH_2O. A deep greenish-brown solution should result.